STATISTICAL AND ALGORITHMIC APPROACHES FOR HEALTH POLICY AND FAIRNESS

A DISSERTATION
SUBMITTED TO THE DEPARTMENT OF BIOMEDICAL DATA SCIENCE
AND THE COMMITTEE ON GRADUATE STUDIES
OF STANFORD UNIVERSITY
IN PARTIAL FULFILLMENT OF THE REQUIREMENTS
FOR THE DEGREE OF
DOCTOR OF PHILOSOPHY

Elizabeth T Chin
April 2022

© Copyright by Elizabeth T Chin 2022
All Rights Reserved

Abstract

Advances in statistics, econometrics, and computer science have the potential to facilitate data-driven decision making in improving the health of populations. However, adapting modern data science methods to eliminate health disparities remains challenging because interventions based singularly on health data do not fully address health issues borne from structural, upstream inequities. A multi-level approach that integrates social and health data to characterize how specific social systems perpetuate health inequities provides opportunities to create more tailored health and social policies. I will discuss examples of addressing health inequity through data science in two contexts: (1) mass incarceration in relationship to public health policies, and (2) algorithmic fairness for structurally vulnerable populations in social policy. An underlying theme is the importance of statistical methodology and study design informed by a holistic understanding of the interplay between social and health systems.

Contents

Abstract **iv**

1 Equity in health policies **1**

1.1 Mass incarceration 1

1.1.1 Decarceration and ongoing risks 1

1.1.2 Social behavioral factors of accepting public health policies 9

1.1.3 Empirical evidence of effectiveness 17

2 Equity in social policies **26**

2.1 Background 26

2.2 Methods 27

2.2.1 Subjectivity in pre-processing 27

2.2.2 Measurement error 28

2.2.3 Model design 28

2.2.4 Evaluation 28

2.3 Results 29

2.3.1 Subjectivity in pre-processing 29

2.3.2 Measurement error 29

2.3.3 Model design 30

3 Methods in precision health **33**

3.1 Gene network rewiring in heart failure 33

3.1.1 Introduction 33

3.1.2 Methods 34

3.1.3 Results 42

3.1.4 Discussion 50

Bibliography **53**

List of Tables

1.1 Persons, Person-Days, and Vaccine Effectiveness 21

List of Figures

1.1 Incarcerated population size and average room occupancy over time 5
1.2 Biweekly participation in labor and other out-of-room activities by age 6
1.3 Adjusted cumulative risk of infection in outbreak prisons 7
1.4 Cumulative vaccine offers 12
1.5 Percentage of Residents Offered Covid-19 Vaccination Who Accepted at Least One Dose 13
1.6 Vaccination acceptance by offer 15
1.7 Vaccination acceptance by offer 22

2.1 Calculating the CalEnviroScreen Score 27
2.2 Percentile versus raw PM2.5 distribution. 29
2.3 Disadvantaged census tracts in San Francisco classified under percentile versus Z-score pre-processing. 30
2.4 Density plots of health metrics estimated from surveys and ER visits. 31
2.5 Discordance between asthma and chronic inflammatory lung disease models. 32

3.1 Gene expression of heart failure and control samples 36
3.2 eQTLs by relevant tissue type 37
3.3 Principal Component Analysis of potential clinical confounders 39
3.4 Dendrograms of heart failure and control networks 40
3.5 Gene prioritization through network topology 41
3.6 Regulatory rewiring of co-expression networks in HF 43
3.7 High quality tissue expression reveals previously undetected cardiac eQTL associations 46
3.8 PPP1R3A knockdown in vitro reveals metabolic regulation in cardiomyocytes. . . . 52

Chapter 1

Equity in health policies

1.1 Mass incarceration

1.1.1 Decarceration and ongoing risks

Background

Over 380,000 incarcerated people in the United States were diagnosed with severe acute respiratory syndrome coronavirus 2 through February 2021, and approximately 2,300 died [10]. Prisons are vulnerable to rapid viral spread, given their population density and the infeasibility of standard distancing measures [80, 65, 78, 100, 105, 112, 123]. Covid-19-related health outcomes appear worse among incarcerated people than in the general population [65, 108, 22].

Correctional systems face difficult trade-offs in their attempts to control Covid-19 transmission. Early releases reduce crowding but may cause public unrest [71]. Curtailing in-prison activities (e.g., work or group therapy) limits mixing but is disruptive and may have adverse health effects [28, 43]. The federal government has issued guidance [12, 9] on measures to reduce Covid-19 transmission in correctional settings, but the recommendations lack specificity and evidence of efficacy. The evidence base in this area remains extremely limited.

The California Department of Corrections and Rehabilitation (CDCR) manages the country's second largest prison system, with 35 institutions that housed 120,000 residents in early 2020. CDCR has undertaken multiple interventions to prevent and contain Covid-19 outbreaks. This study describes how CDCR's incarcerated population has changed during the pandemic, focusing on room occupancy and participation in out-of-room activities. For prisons that have experienced outbreaks, we estimate the extent to which those two factors are associated with Covid-19 infection rates.

Data

CDCR provided data on all incarcerated people aged $\geq$ 18 years residing in its prisons during the period March 1 through October 10, 2020. The data were provided at the person-day-level, which allowed daily tracking of changes in any time-varying information until residents' release or death.

The data included variables indicating residents' demographic (sex, age, and race or ethnicity) and health characteristics; location; participation in prison labor, education, and other activities; and Covid-19 testing history. The data contained each resident's security level (1 [lowest] to 4 [highest]) which determines housing locations and eligibility for work and other activities [4]. Locational information specified the room in which each resident spent the night. Rooms were defined as discrete spaces, at least partially enclosed by solid walls, and were classified as cells or dormitories of varying sizes.

The health information included indicators for diagnosed medical conditions and Covid-19 risk score. This score, developed by CDCR, is an integer-based estimate of each resident's probability of severe health outcomes following Covid-19 infection. Scores correspond to the presence of demographic and clinical characteristics identified in the literature as risk factors for severe Covid-19-related illness, and CDCR considers scores ≥ 3 to indicate high-risk (Table S1).

Testing information included dates and results. CDCR has been testing residents using real-time PCR and antigen tests since April 2020. Testing expanded during the study period, eventually employing both reactive mass testing and periodic surveillance testing. Prisons experiencing large outbreaks tested residents at particularly high rates. By Fall 2020, all prisons were testing 5-25% of residents every two weeks.

We created variables to describe risk factors for Covid-19 exposure and transmission, based on residents' housing situation and their participation in out-of-room activities. With respect to housing, we calculated the daily number of residents housed in each room (square footage of rooms was unavailable). This count variable had a bimodal distribution, with many residents living alone or with one other resident, or in substantially larger rooms ($\geq$ 10 residents), and relatively few in between. For some analyses we dichotomized this variable, distinguishing residents in "cells" (1-2 occupants) and "dormitories" ($\geq$ 3 occupants); this aligned with CDCR's conception of the major division in room sizes.

With respect to activities, the resident-day-level data included information on residents' out-of-room participation in labor (e.g., janitorial), education (e.g., high school classes), and other activities (e.g., religious services) [11, 8]. From April 2020, educational activities were confined to residents' rooms. Consequently, we focused on labor and other out-of-room non-educational activities excluding recreation and meals which were not comprehensively tracked. We specified variables indicating whether each resident participated in each activity type and variables indicating whether each resident or a roommate did so in the previous two weeks.

Finally, we classified prisons into 5 categories based on the predominant resident security levels,

housing configurations, and CDCR advice: reception centers, medical prisons, low security and general population prisons, high security prisons, and mixed security and medium security prisons.

Methods

We calculated changes over the study period in the size and composition of the incarcerated population, in housing, and in participation in out-of-room activities.

We used person-level survival analysis to estimate the association between room occupancy and labor activities, respectively, and rates of Covid-19 infection. We focused on sustained within-prison transmission, therefore limiting the analysis to prisons with outbreaks involving substantial resident-to-resident spread. We defined prisons with outbreaks as those having ≥ 50 cumulative cases during the study period and ≥ 10 incident cases detected on at least one day in that period. We defined an outbreak's start date as 14 days prior to the first day with ≥ 10 incident cases.

We specified several additional prison-level and resident-level eligibility criteria for the survival analysis. Briefly, to allow ≥ 90 days follow-up, we excluded prisons (n=7) with outbreaks that began after July 12, 2020; to minimize confounding, we excluded one prison with testing rates that differed substantially between cells and dormitories; and we excluded prisons (n=3) whose outbreaks were seeded by mass introduction of cases (e.g., San Quentin), because their epidemic growth may have been atypical. Within eligible prisons, we included residents present on the day the outbreak began who were tested for Covid-19 at least once during the 90-day period.

The observation period for eligible residents' observation ran from the start of their prison's outbreak until the sample collection date of their first positive test or their last negative test. Release or transfer to another prison were also censoring events.

We fit a multivariable Cox proportional hazard regression model to estimate the associations of interest. The outcome variable indicated the sample collection date for the first positive Covid-19 test result among residents who had a positive test. The main exposure variables were room occupancy at the outbreak start and room-level labor participation during the 14-day period prior to the outbreak start. We also included prison fixed effects. We assessed the appropriateness of the proportional hazards assumption by inspecting plots of Schoenfeld residuals.

We conducted sensitivity analyses. Because there may be systematic differences in how residents with higher Covid-19 risk scores or higher security levels mix with other residents, we added baseline values of these covariates. We varied the required follow-up period for prison inclusion. We allowed the observation period for residents who did not test positive, exit the prison, or die to extend to the end of the study period, regardless of their last negative test date. We estimated the model clustering standard errors at the room and prison levels.

Results

From March 1 to October 10, 2020, the resident population of California prisons decreased from 119,401 to 96,623 (Figure 1.1), a reduction of 19.1% that reversed prior trends [5]. High security prisons (7.0%) and medical prisons (14.4%) had the smallest relative reductions.

On October 10, 2020, 96.7% of residents were male and 11.5% were aged 60 years or older. Nearly three-quarters were Hispanic (44.5%) or non-Hispanic Black (29.5%). Forty percent had at least one medical condition, and 18.3% had a Covid-19 risk score of ≥ 3. The average number of residents per room decreased from 20 to 10. However, seven prisons still averaged ≥ 20 occupants per room in October 2020, and 25 had ≥ 1 room with ≥ 20 occupants. The proportion of residents in dormitories decreased from 37.1% to 30.9%, though a substantial fraction of higher risk residents were still housed in dormitories.

By October 10, 81.8% (79,046) of still-incarcerated individuals had been tested for Covid-19 at least once, and a total of 96,440 residents including those released between March and October had been tested. Of the 96,440 residents, 15,162 were positive; 13,636 of these cases resolved by October 10—3.2% were hospitalized, 0.3% were in intensive care units, and 0.5% died. Severe Covid-19 outcomes were most likely for older and higher risk residents.

Participation in out-of-room activities other than labor decreased precipitously between March and April 2020 and remained low through October. However, labor participation decreased only slightly during the study period (Figure 1.2). The lowest levels of and the largest decreases in labor participation were among residents aged ≥ 80 years, but more than 10% of residents in this age group and more than 20% of 70-79 year-olds were still participating in labor in October. These labor participation results were generally consistent according to resident risk measures, prison types, and outbreak history.

In the nine prisons with outbreaks that met our eligibility criteria for the multivariable risk analysis, 21,750 eligible residents living in 6,928 rooms were tested at least once. Over 90 days, the cumulative percentage of each prison's population tested ranged from 21.3 to 99.9%, and the cumulative percentage of each prison's population confirmed positive ranged from 2.4 to 45.1%.

Rates of Covid-19 infection among residents of dormitories (≥ 3 occupants) were more than double those among residents of cells (Adjusted hazard ratio [AHR], 2.51; 95% Confidence Interval [CI], 2.25-2.80; p¡0.001) (Figure 1.3). Residents of rooms with occupants participating in out-of-room labor also had higher rates of infection compared to those without participation (AHR, 1.56; 95% CI, 1.39-1.74). These differences represent a cumulative risk of infection that is 28.6 percentage points higher (95% CI, 16.7-30.6%; 62.1% vs. 33.4%) for dormitories compared to cells, and 13.1 percentage points higher (95% CI, 12.8-13.3%; 53.7% vs. 40.6%) for rooms with labor participation than for rooms without it. Estimates proved fairly robust in sensitivity analyses. While, in theory, residents with higher Covid-19 risk scores may take greater precautions to avoid more severe consequences from infection, analyses that included this variable did not detect an association with lower risks.

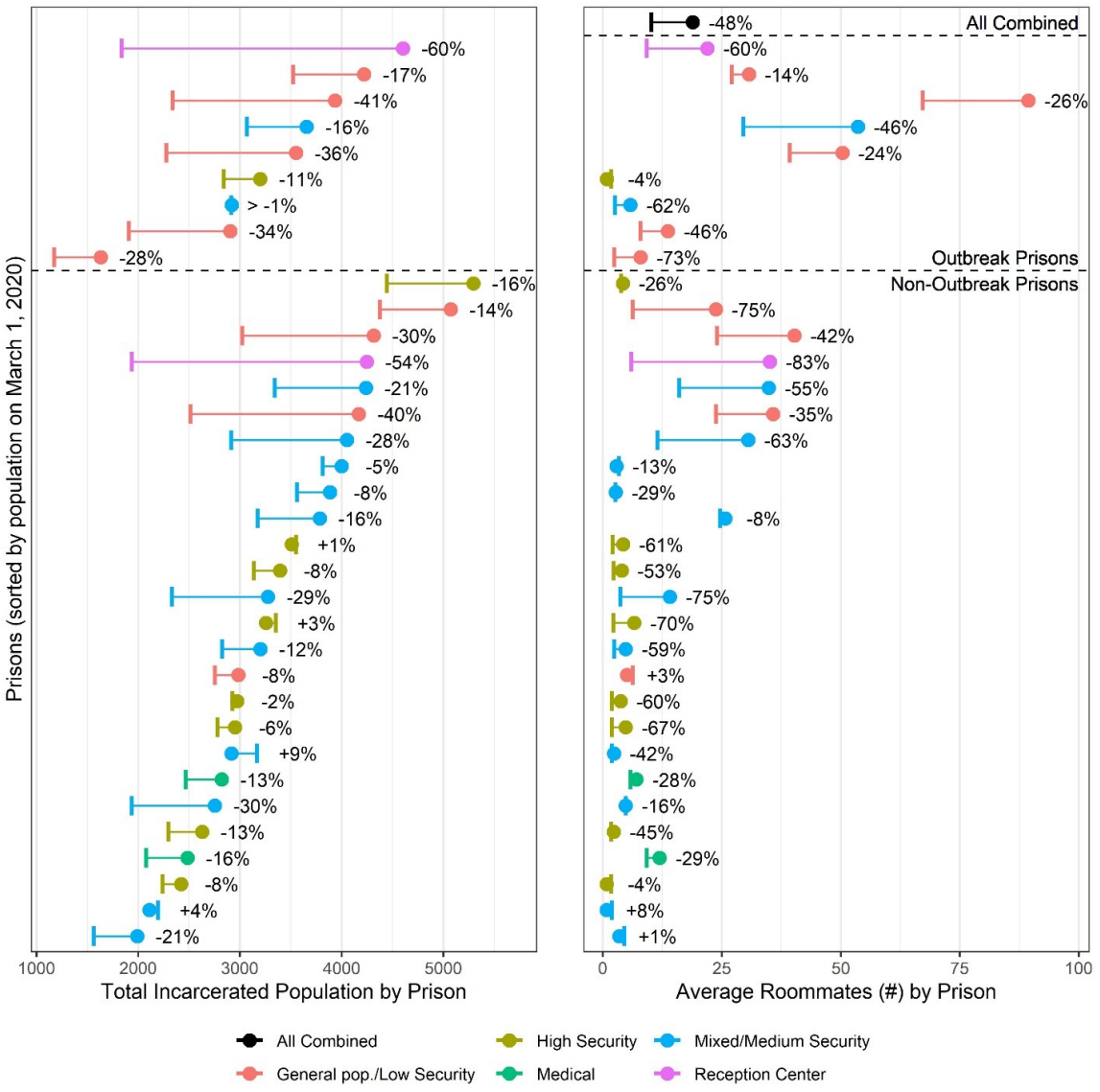


Figure 1.1: Incarcerated population size and average room occupancy over time. Graph shows the change in total prison population size (left) and change in the average number of roommates an individual in that prison has (right), for each of the 35 prisons, color-coded by prison type, and for all prisons combined in black (only right panel), from March 1, 2020 (filled circle) to October 10, 2020 (vertical bar). The outbreak prisons used in the multivariate risk analysis are shown above the dashed line, and remaining prisons are shown below the dashed line.

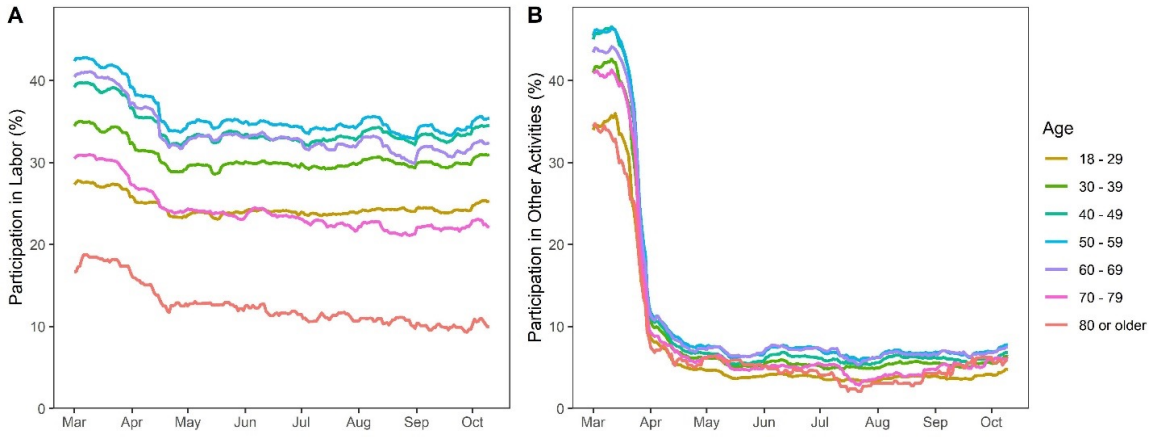


Figure 1.2: Biweekly participation in labor and other out-of-room activities by age. Graph shows rolling average participation in activities, defined as whether an individual participated in labor or other activities with at least one other person during any day in the past 2 weeks. Panels show (A) labor participation by age; (B) other participation by age. Data cover all prisons from March 1, 2020 through October 10, 2020.

Discussion

Over a 7-month period following the onset of the Covid-19 pandemic, the resident population of California state prisons decreased by one-fifth and room occupancy halved. However, many medically vulnerable residents remained incarcerated, and a substantial proportion of them continued to live in dormitory housing and participate in work activities that involved mixing. In nine prisons that experienced large outbreaks, we found that residents living in rooms with ≥ 2 others had a 2.5-fold higher infection rate and that residents in a room whose occupants participated in out-of-room work had a 1.6-fold higher rate. Since the pandemic began CDCR has taken drastic steps to mitigate transmission and stem outbreaks. Nonetheless, as of February 13, 2021, there had been 48,758 confirmed cases among residents and 205 deaths. These represent substantially higher rates of infection and mortality that state's general population has experienced.

The patterns we observed suggest opportunities for further risk reduction. The substantial numbers of older and higher-risk residents who continue to live in high occupancy rooms is an important target group for prevention efforts. Members of those high-risk groups who participate in group activities, or who share a room with others who do, are also an important target group.

Our results are consistent with key messages from the limited evidence base on respiratory infections in incarcerated populations [80, 65, 78, 100, 105, 112, 123, 108, 22, 71, 28, 43, 83, 90, 96]. The interconnected nature of the residents of congregate institutions means that outbreaks, especially those that penetrate higher occupancy rooms, can quickly become building or prison outbreaks. Correctional facilities, nationally and internationally, should redouble efforts not only to

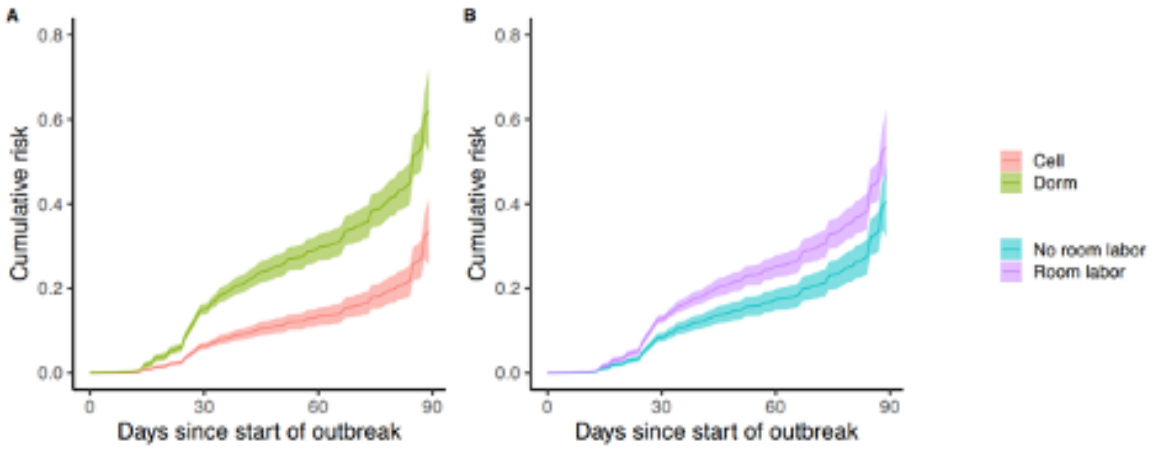


Figure 1.3: Adjusted cumulative risk of infection in outbreak prisons. Graphs show the adjusted marginal cumulative risk of infection over 90 days from the start of a prison outbreak for (A) room type and (B) room labor (i.e., whether anyone in the room participated in out-of-room labor). Data includes 90 days follow-up for 9 prisons.

prevent outbreaks but also to increase protective measures taken for their large, medically vulnerable subpopulations, including further reductions in the density of living arrangements [125].

Our access to person-level, daily data from a large prison system with high rates of testing created analytical opportunities that recent studies of Covid-19 in incarcerated populations have not had, including minimizing biases from selection into testing, However, our study also had limitations. First, we could not identify networks of specific contacts, a limitation that is likely to have mattered most to our estimates of the effect of labor participation. Second, we used room occupancy to indicate in-room contacts because density measures (e.g., residents per square foot) were not available. The most plausible effect of misclassifying room exposures would be to bias to the null our estimates of the effect of living in higher occupancy rooms. Third, we lacked information on some potential exposures, such as contacts with staff and during meals in common areas. Finally, although CDCR undertook extensive testing, not all residents were tested and test frequency varied across institutions. If residents of dormitories or of rooms with labor participation were tested relatively frequently, or testing there more precisely targeted infected residents, our estimates of these factors on infection risk may be biased upward.

Prisons remain particularly dangerous settings for Covid-19-related morbidity and mortality. Our study shows that thousands of vulnerable incarcerated people continue to be housed in settings where their risk of Covid-19 infection is high. Protective measures such as decarceration, testing, vaccination, and efforts to enhance vaccine uptake remain vital [45]. Residents at greatest risk of transmission and infection, such as those living dormitories and participating in labor, should be prioritized. Furthermore, as correctional systems offer vaccination to residents, our study highlights

the importance of prioritizing both those at highest risk of adverse outcomes following infection and those most likely to contract and spread the virus.

1.1.2 Social behavioral factors of accepting public health policies

Background

The Covid-19 pandemic has ravaged prisons and jails. To date, nearly 400,000 cases and 2,500 deaths have occurred among incarcerated people in the United States (U.S.) alone [14], with case and mortality rates that far exceed those in the general community [69]. The infeasibility of key non-pharmaceutical interventions (e.g., social distancing) for preventing transmission helps explain the elevated risk, as does the high prevalence of chronic diseases in this population [41] . The Centers for Disease Control and Prevention has recommended that incarcerated people be prioritized for Covid-19 vaccines [2], but states are taking different approaches [82]. A few states began implementing vaccination programs in correctional institutions as soon as vaccines became available, and have already offered doses to many residents; other states have not yet begun offering vaccinations in these settings [82, 77]. Vaccine hesitancy is common in jails and prisons, in part because of limited access to information and widespread mistrust of correctional authorities and the medical providers [29]. Racial and ethnic minorities, a majority of many incarcerated populations, are disproportionately unlikely to accept vaccination and other medical interventions. The high threshold for achieving herd immunity in prisons and jails amplifies the risks associated with under-vaccination [102]. California prioritized incarcerated people for Covid-19 vaccination. The California Department of Corrections and Rehabilitation (CDCR), which operates the country's second largest state prison system, launched a vaccination program for residents in late 2020 and scaled it up rapidly. We tracked the program's rollout, focusing on the proportion and characteristics of residents who accepted vaccine offers.

Methods

Vaccination program

CDCR launched its program on December 22, 2020, in three prisons with the largest medically vulnerable populations. Rollouts at other prisons followed, with the last prison commencing vaccinations on January 19, 2021. Within prisons, the criteria CDCR used to prioritize residents for vaccination changed over time as vaccine shipments arrived and new state and federal guidances were issued. The prioritization criteria variously included residency in a specialized medical or psychiatric care settings, risk factors for severe outcomes from Covid-19, no confirmed SARS-CoV-2 infection (or none in the previous 90 days), employment in a high-contact job, and due dates for a second dose.

Residents received one of the two vaccines (Pfizer-BioNTech or Moderna) authorized for emergency use in the U.S. at the time of our study period, December 22, 2020, through March 4, 2021. Vaccination was voluntary, and residents were permitted to decline without sanction. Prison healthcare staff recorded whether each vaccine dose offered was accepted or declined. Residents who

declined a vaccine dose were eligible to be re-offered one at a later time.

Data and Variables

CDCR provided person-level data on residents' demographic and clinical characteristics, housing, and Covid-19 testing history. The demographic information included sex, age, race, and ethnicity. We grouped the race and ethnicity information, which came from a combination of self-reports and administrative records, into categories used by the U.S. Census Bureau (Hispanic, non-Hispanic Black, non-Hispanic White, non-Hispanic American Indian/Alaska Native, non-Hispanic Asian/Pacific Islander, and non-Hispanic Other) [1].

CDCR developed a Covid-19 risk score to grade residents' likelihood of severe Covid-19-related disease. This risk score sums weighted values for 17 items identified in the scientific literature as risk factors for severe outcomes following SARS-CoV-2 infection (Table S1). We categorized scores into "low" risk (scores of 0 and 1), "medium" risk (2 and 3), and "high" risk (> 4).

The data also included Covid-19 testing information. CDCR has undertaken extensive testing of residents for SARS-CoV-2 since April 2020, using real-time PCR and antigen tests [41]. We defined prior SARS-CoV-2 infection as having had at least one positive test while in CDCR custody.

In addition, the data included various carceral characteristics with potential relevance for vaccine acceptance—particularly, security level, room type, and participation in penal labor. CDCR rates each resident's security level from 1 (lowest) to 4 (highest), based on a multifactorial assessment of the resident's risk of misconduct; this rating influences housing placement and eligibility for activities such as visitations, recreation, and penal labor. Residents are housed in rooms, discrete spaces that are at least partially enclosed by solid walls. We defined room type according to the number of residents housed in each room, dichotomizing this variable into cells (rooms with 1-2 occupants) and dormitories (> 3 occupants). Finally, using information on residents' participation in work roles (e.g., janitorial, food preparation), we created a binary variable indicating whether each resident had participated in penal labor within the prior 14 days.

Statistical Analysis

We calculated the proportion of residents who accepted first and second vaccine doses among residents offered those doses ("offerees"). We also calculated patterns of acceptance among residents who were re-offered vaccines after previously declining them ("re-offerees").

We used multivariable logistic regression analysis to identify demographic characteristics associated with vaccine acceptance at the resident level. In the primary analysis, the outcome variable distinguished offerees who accepted > 1 vaccine doses from offerees who did not accept any doses. The four predictors of interest were age group (18-39 years, 40-64 years, > 65 years), racial or ethnic group, Covid-19 risk score, and prior SARS-CoV-2 infection. The model included prison fixed effects and adjusted for residents' security level, room type, and participation in penal labor. Time-varying

variables were assigned their values on the date of the offeree's first offer.

A secondary analysis focused on re-offerees followed the same general form as the primary analysis, except the analytic sample was restricted to re-offerees. The outcome variable distinguished re-offerees who accepted > 1 subsequent offer from those who did not. We report predicted margins from all analyses.

Our analyses did not adjust for sex because male and female residents were housed in separate prisons, making a sex variable perfectly collinear with the prison fixed effects. To test the robustness of our main results to this omission, we re-ran the primary analysis separately for male and female offerees. Additional details regarding model and variable specifications are provided in section II of the Supplementary Appendix.

Analyses were performed using R software, version 3.5.2 (R Foundation for Statistical Computing). We performed post hoc Bonferroni correction for the primary and secondary outcomes to account for multiple comparisons (14 for each of the primary and secondary analyses) by estimating 99.6% confidence intervals instead of 95% confidence intervals.

Results

Vaccine Offers A total of 97,779 people spent at least one night in a CDCR prison during the study period. CDCR's vaccine program scaled up quickly, with 8% of residents offered at least one vaccine by the end of the first month, 37% by 6 weeks, and 60.1% by 2 months (Figure 1.4). By March 4, 2021, CDCR had offered 66.1% (64,633/97,779) of residents a first dose and 23.9% (23,413/97,779) first and second doses.

Characteristics of Vaccine Offerees Most of the 64,633 offerees in our sample were male (95.6%), younger than 65 years (92.0%), and Hispanic (42.0%) or Black (31.7%). Approximately one quarter of offerees participated in penal labor (28.8%), lived in dormitories (25.8%), and had a prior SARS-CoV-2 infection (27.8%).

A substantial proportion of offerees were at risk for severe outcomes from Covid-19 infection. One third had medium or high Covid-19 risk scores, and more than half had at least one medical condition linked to increased risk of severe Covid-19-related illness. The most common pre-existing conditions were obesity or severe obesity (40.7%), chronic kidney disease (16.1%), diabetes (9.2%), and cardiovascular disease (4.5%).

Vaccine Acceptance Two thirds of offerees (42,952/64,633) accepted one or both doses. The proportion who accepted was very similar among male (66.6%; 41,145/61,820) and female (64.2%; 1,807/2,813) offerees.

The proportion of offerees that accepted a first dose decreased during the study period, from 77.2% in the first month to 63.6% in the last month. Among residents who accepted a first dose and were offered a second, 98.7% accepted; this proportion increased from 89.1% in the first month to 98.7% in the last month.

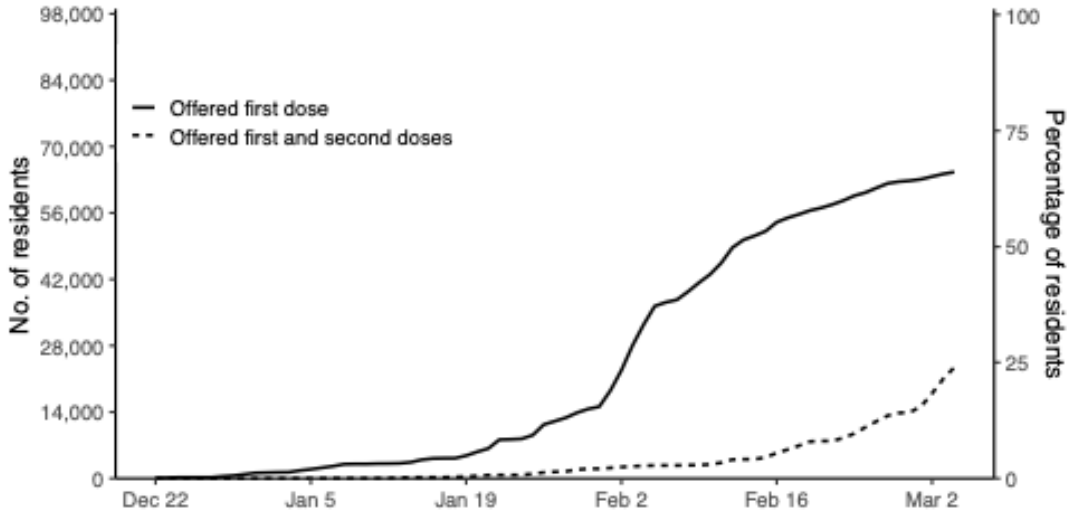


Figure 1.4: Cumulative offers of Covid-19 vaccinations to residents of California state prisons, December 22, 2020, through March 4, 2021.

Adjusted analyses estimated similar levels of acceptance of one or more doses among offerees who did (67.4%; CI, 66.3-68.4%) and did not (66.2%; CI, 65.6-66.8%) have prior SARS-CoV-2 infection (Figure 1.5). But there was wide variation in acceptance according to race or ethnic group. Acceptance was highest among Hispanic offerees (72.4%; CI, 71.7-73.1%) and White offerees (71.9%; CI, 70.7-73.1%). Acceptance was slightly lower among American Indian/Alaska Native offerees (67.5%; CI, 62.6-72.3%) and Asian/Pacific Islander offerees (67.5%; CI, 63.3-71.8%), and substantially lower among Black offerees (54.7%; 99.6% Confidence Interval, 53.8-55.7%).

Acceptance was positively associated with older age and higher Covid-19 risk score. Offerees aged 18 to 39 years (58.0%; CI, 57.2-58.8%) and 40 to 64 years (73.4%; CI, 72.6-74.1%) were less likely to accept a vaccine dose than offerees aged 65 years or older (84.5%; CI, 82.6-86.4%). Offerees with low (61.6%; CI, 60.9-62.2%) and medium (74.0%; CI, 72.9-75.1%) Covid-19 risk scores were less likely to accept a vaccine dose than offerees with high Covid-19 risk scores (82.5%; CI, 81.1-83.9%).

The race and ethnic disparities reported above were very consistent across Covid-19 risk score and age groups, such that acceptance levels among Black offerees with high Covid-19 risk scores were similar to those among White and Hispanic offerees with low Covid-19 risk scores and American Indian/Alaska Native and Asian/Pacific Islander offerees with moderate Covid-19 risk scores (Figure S1). Acceptance levels among Black offerees in the youngest age group and Black offerees with low Covid-19 risk scores were below 50%.

Vaccine Acceptance among Initial Decliners Overall, 8.7% (1,962/22,582) of residents who declined a first dose offer received at least one re-offer; 45.9% (901/1,962) of those re-offerees accepted

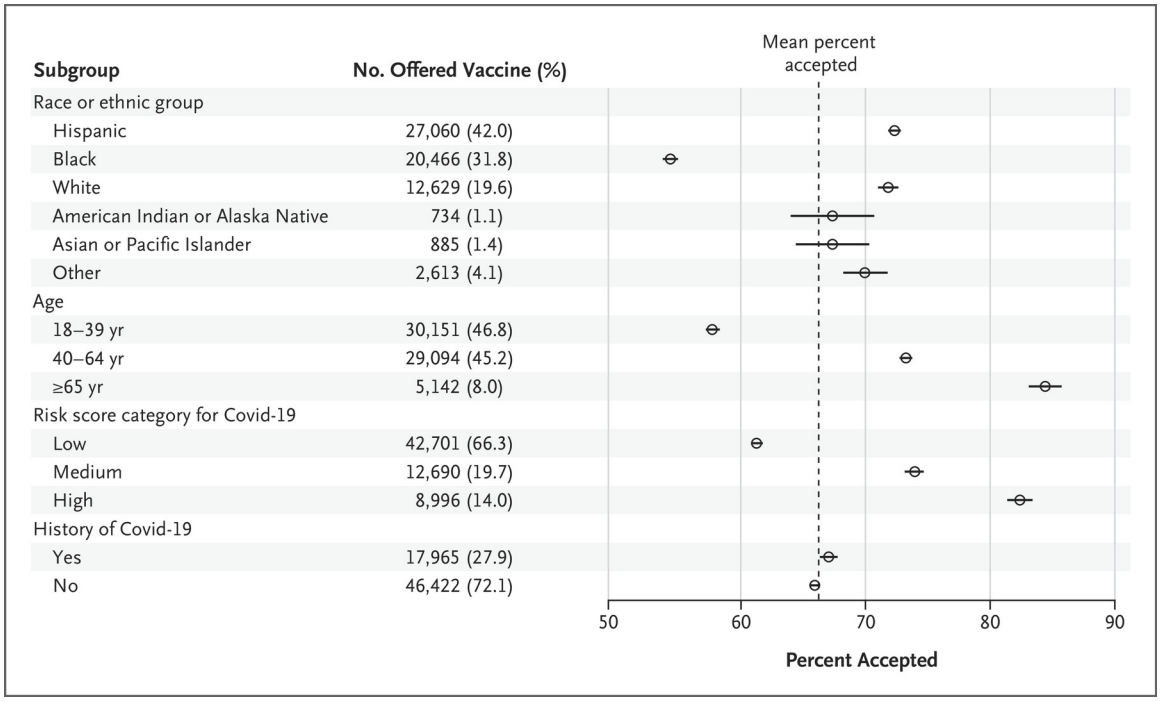


Figure 1.5: Percentage of Residents Offered Covid-19 Vaccination Who Accepted at Least One Dose. Shown are the predicted margins estimated from the results of multivariable logistic-regression analyses of the sample of 64,387 incarcerated residents who were offered at least one dose of the BNT162b2 or mRNA-1273 vaccine, with adjustments for room type (defined according to the number of residents housed in a room), participation in penal labor, security level, and prison. All the categories of race or ethnic group other than Hispanic indicate non-Hispanic residents. The California Department of Corrections and Rehabilitation (CDCR) developed a risk score to grade residents' likelihood of severe Covid-19–related disease. The risk score sums weighted values for 17 items identified in the scientific literature as risk factors for severe outcomes after SARS-CoV-2 infection (Table S1). We categorized scores into low risk (score of 0 or 1), medium risk (2 or 3), and high risk (≥ 4). Residents were considered to have had a history of Covid-19 if they had had a positive test result while in CDCR custody, before the date of the first offer of a vaccine.

(Figure 1.6). Most of these acceptances were in response to a first re-offer. The proportion of re-offers that were accepted decreased with each subsequent re-offer.

Adjusted analyses of acceptance among re-offerees did not show significant differences according to race or ethnic groups. However, younger and healthier re-offerees were more likely to accept. Specifically, re-offerees aged 18 to 39 years (47.6%; 95% CI, 43-52.3%) or 40 to 64 years (48.7%; 95% CI, 44.1-53.2%) were more likely to accept than re-offerees aged 65 years or older (33.4%; 95% CI, 24.3-42.5%). Similarly, re-offerees with low (49.3%; 95% CI, 45.3-53.3%) or medium (47.3%; 95% CI, 40.9-53.6%) Covid-19 risk scores were more likely to accept than re-offerees with high Covid-19 risk scores (38.1%; 95% CI, 31.1-45.1%).

Sensitivity Analysis Separate analyses for male and female offerees showed similar results, with two notable exceptions. Among female offerees, Hispanic women and women with prior Covid-19 infection were less likely to accept than White women and those with no prior infection, respectively.

Discussion

This study of vaccine acceptance among residents of California state prisons found that two thirds of those offered vaccines accepted at least one dose. Acceptance was relatively low among non-Hispanic minorities, especially Black residents and residents at lower risk of severe illness from Covid-19. However, nearly half of residents who were re-offered a first vaccine dose after initially declining accepted it.

Calculating levels and patterns of vaccine acceptance in the general community is currently challenging for several reasons. Denominators for acceptance rates are elusive as eligibility rules change and people queue for appointments. Many eligible people may not get vaccinated because they are unaware of their eligibility or face access barriers rather than being truly reluctant. In addition, important information on who has been vaccinated, including race and ethnicity, is incomplete [26]. Studying acceptance in circumscribed settings, such as prisons, mitigates these challenges.

Long-term care facilities are also circumscribed settings and provide a relevant comparator. A recent study of 12,702 skilled nursing facilities enrolled in the Pharmacy Partnership for Long-Term Care Program found that the median estimated percentage of residents vaccinated per facility was 77.8% [58, 59]. Although this is more than 10 percentage points higher than the overall acceptance levels in the incarcerated population we studied, it is quite close to the acceptance levels we observed among older and more medically vulnerable residents.

The substantially lower acceptance observed among Black, younger, and healthier offerees is consistent with both survey evidence of willingness to obtain vaccination [7, 99, 57] and preliminary data on vaccine uptake in the general community [3]. Greater reluctance among those at lower risk of severe disease is predictable, but in congregate settings, where transmission risks and herd immunity thresholds are high [102], low vaccination rates in any subgroup ensure continuing risks.

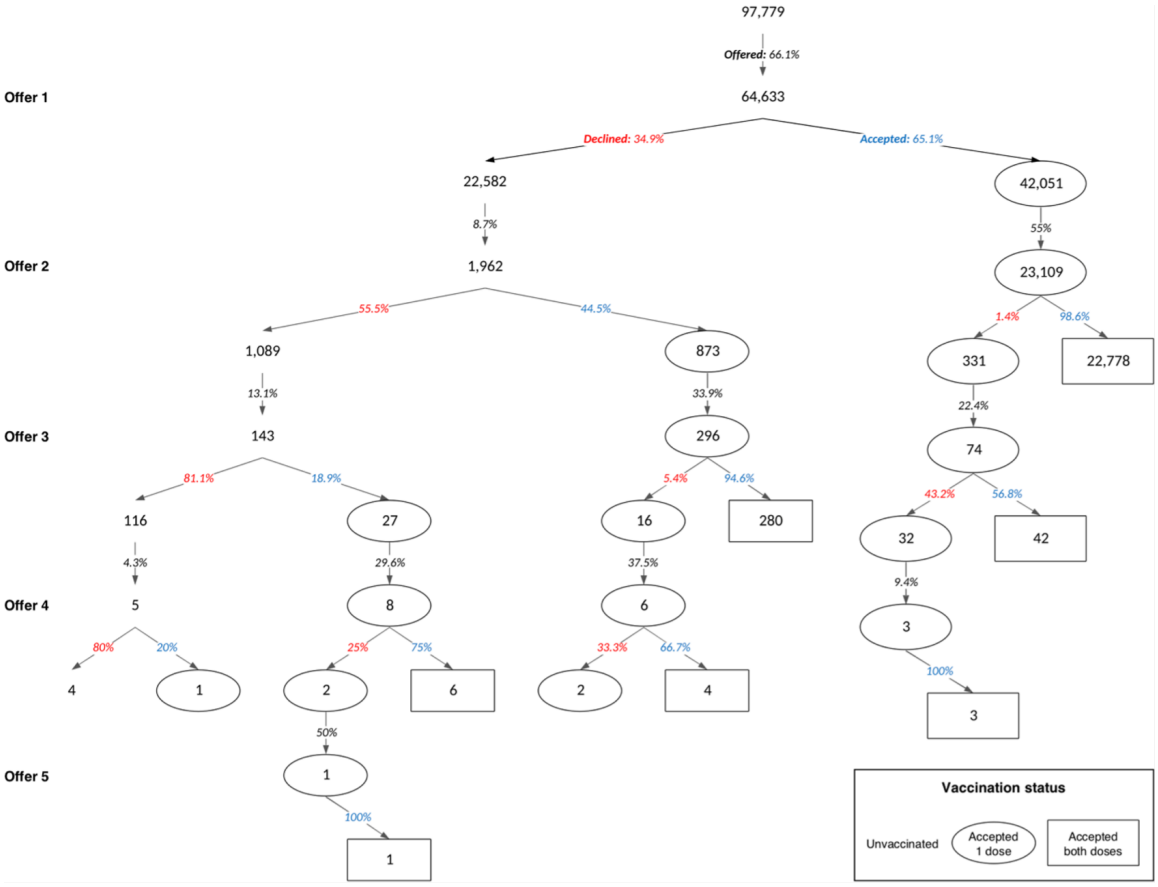


Figure 1.6: Vaccination acceptance by offer. Nodes indicate the number of residents at each offer number. The percentages indicate offers (black), declines (red), and acceptances (blue).

The considerable vaccine hesitancy we observed among Black residents is particularly troubling. One plausible explanation is mistrust [95]. The adverse effects of historical exploitation and persistent disparities in medical care on minorities' trust in providers and care seeking behaviors have been well documented [23, 73, 104, 36, 101]. Medical mistrust appears to be particularly high among African American men [23, 32, 30].

Hispanic offerees in our sample had similar levels of vaccine acceptance to white offerees. This finding matches results from survey research in the general community regarding intentions to obtain a Covid-19 vaccine [89], but conflicts with growing evidence of relatively low uptake among Hispanics [3, 106]. Lower access barriers in prisons than in the general community may explain the discrepancy.

Our finding that a large proportion of residents who initially declined a first-dose offer later accepted a re-offer indicates that hesitancy is not always fixed. Younger and healthier residents were especially likely to switch. Why residents switched is not clear. As the number of vaccinated co-residents climbed, peer pressure may have played a role; so might the reassurance of witnessing no ill effects among vaccinated co-residents. Regardless, these results suggest re-offers have real potential to boost vaccine coverage.

This study has several limitations. First, we report levels and patterns of hesitancy in the first 10 weeks of CDCR's program; these statistics may change as the number of vaccinated residents grows, knowledge improves, and vaccine options expand. CDCR began offering Johnson & Johnson's one-dose vaccine after our study period ended. Relatedly, the results reflect offers made to a non-random selection of residents, many of whom were prioritized based on risk factors for severe disease. Acceptance levels are likely to be lower in the remaining one third of residents, who generally have lower risk. Second, results from our re-offer analyses should be interpreted with caution because a majority of those who declined had not received re-offers at the time of our data extract, and those to whom re-offers were made were not selected systematically. Third, residents' peer interactions are likely to have had a strong bearing on their propensity to accept vaccine offers; although we adjusted for prisons and room size, we did not measure those finer environmental influences. Fourth, we did not have access to detailed information on the procedures by which vaccine offers were made at each prison nor why residents declined. Finally, the generalizability of our results to other prisons or non-incarcerated populations is unknown.

Correctional settings are high-risk settings for Covid-19-related spread, morbidity, and mortality. More incarcerated people have died from Covid-19 in U.S. correctional facilities in the last year than died by capital punishment in the last 70 years [58, 53, 13]. Vaccines are a critical means for controlling these risks. The substantial degree of vaccine uptake in California prisons promises major preventive health benefits. Even greater benefits will accrue if the vaccination program can be buttressed with successful efforts to build trust and reduce hesitancy, particularly among non-Hispanic minorities and younger residents.

1.1.3 Empirical evidence of effectiveness

Background

The BNT162b2 (Pfizer-BioNTech) and mRNA-1273 (Moderna) vaccines appear highly effective in preventing severe acute respiratory syndrome coronavirus 2 (SARS-CoV-2) infection and coronavirus disease 2019 (COVID-19) illness. Augmenting efficacy evidence from clinical trials [18, 21], observational studies among healthcare workers [119, 25], adults aged 65 years or older [117], and the general community [63, 15] have reported levels of protection from full vaccination ranging from 89% to 95%. However, except for two relatively small studies of partial vaccination in skilled nursing facilities [37, 34], no published studies to date have examined the effectiveness of COVID-19 vaccines in congregate settings, where risks of transmission are very high.

Prisons and jails are especially risky congregate settings. Living quarters are often densely populated and poorly ventilated, physical distancing is typically infeasible, and pre-existing medical conditions associated with severe COVID-19 illness are prevalent among incarcerated people [42, 46]. Recognizing these risks and the considerable potential for vaccines to reduce them, approximately half of US states have prioritized incarcerated people for COVID-19 vaccines. In contrast, [24] states have not included incarcerated people in vaccine distribution plans or have assigned them to lowest priority tiers.[91, 115]

The California Department of Corrections and Rehabilitation (CDCR), which operates the second largest state prison system, launched a COVID-19 vaccination program on December 22, 2020, and rapidly scaled up the program across its 35 prisons.[40] CDCR has conducted extensive testing and collected detailed data relevant to COVID-19 risks, interventions, and outcomes. We analyzed these data to estimate effectiveness of mRNA vaccines against confirmed SARS-CoV-2 infection among nearly 61,000 incarcerated people in California.

Methods

Study design and population

We conducted a retrospective cohort study spanning the 70-day period from December 22, 2020, through March 1, 2021, during which residents were offered either BNT162b2 or mRNA-1273 vaccines. Prioritization criteria CDCR used to direct first-dose offers changed over time as supply expanded and state and federal guidance evolved. Criteria included residency in a specialized medical or psychiatric care setting, age and medical comorbidities, no confirmed SARS-CoV-2 infection (or none in the previous 90 days), and participation in penal labor. CDCR prioritized timely second-dose offers to adhere to recommended dosing schedules.

Residents were eligible for inclusion in the study cohort if they were incarcerated in a CDCR prison on the study start date and had no prior confirmed SARS-CoV-2 infection. Cohort members contributed observation time beginning on the study start date and ending on the day of the earliest

of the following events: release from CDCR custody, sample collection for a positive SARS-CoV-2 diagnostic test, or study end date.

Data and key measures

CDCR collects and stores daily data on each resident. Data provided for this study included demographic characteristics (sex, age, racial or ethnic group), documented history of 25 comorbid conditions (e.g., hypertension, chronic kidney disease, asthma), and a composite COVID-19 risk score. CDCR designed the COVID-19 risk score to grade risks of severe illness from SARS-CoV-2 infections based on individual demographic and clinical information, and the agency has used this score to guide COVID-19 mitigation policies, including prioritization of testing and vaccination. We also obtained person-day level variables indicating each resident's prison, facility, building, housing unit, floor, and room of residence; room type (cell or dormitory); security level; and participation in penal labor.

Detailed SARS-CoV-2 testing information came from a multilayered resident testing program that included risk-based routine testing, surveillance testing, and testing in response to detected outbreaks. Information provided on accepted vaccine doses allowed us to classify cohort members' daily vaccination status into six categories: unvaccinated, from 0 to 6 days after receiving a first dose, from 7 to 13 days after a first dose, from 14 days after a first dose until receipt of a second dose, from 0 to 13 days after a second dose, and from 14 days after a second dose.

To obtain a measure of risk of infection from correctional staff, we constructed a prison-day level variable comprising the rolling 7-day COVID-19 case rate among staff at each prison. Infections among correctional staff were identified through a program of regular SARS-CoV-2 testing, mandated and administered by CDCR.

Statistical analysis

To obtain estimates of vaccine effectiveness, we fit multivariable models using the Andersen–Gill extension of the Cox proportional hazards model [24] to account for time-varying covariates using person-day level data. The primary outcome of interest was SARS-CoV-2 infection, confirmed by positive PCR or antigen test. We specified exposure status according to the six vaccination categories described above. Effectiveness estimates are expressed as 1 minus the hazard ratio.

Analyses adjusted for residents' racial or ethnic group, COVID-19 risk score, security level, room type, participation in penal labor, staff case rate, and prison (fixed effects). We did not adjust for sex because men and women are generally housed in separate prisons, making this variable highly collinear with prison. To account for non-independence between cohort members, we clustered standard errors by housing unit. Housing units are discrete cohorts within prisons, consisting of residents who co-participate in activities (e.g., recreation, laundry, dining).

Secondary analyses

We conducted four sets of secondary analyses. First, we estimated effectiveness in two subgroups of interest. Specifically, recognizing that our primary analysis mixes effects of two different vaccines, we ran one subgroup analysis focusing on mRNA-1273 vaccinations only (which accounted for 78% of all first doses and 72% of all doses administered in the study period). We also estimated effectiveness among medically vulnerable residents by restricting the analytic cohort to residents with COVID-19 risk scores of 2 or higher, indicating moderate or high risk. Residents with COVID-19 risk scores of 2 or higher were either aged 65 years and older or younger than 65 years with comorbid conditions associated with severe COVID-19 disease.

Second, we estimated effectiveness in a broader population that included residents with prior infections and those who entered prison during the study period. Third, we examined the sensitivity of our effectiveness estimates to alternative model specifications, including censoring observation time at the collection date of cohort members' last test (to exclude time periods in which infection status was unknown), and computing cluster-robust variance estimators with clusters defined at various levels (prison, facility, building, housing unit, floor, room, and person). Finally, to assess the sensitivity of estimates to choice of study period, we re-estimated effectiveness using a series of alternative study end dates between February 15 and July 1, 2021.

Results

Sample characteristics and vaccination uptake

60,707 residents met the cohort inclusion criteria and were followed for an average of 57.6 days (median, 70 days). By February 1, 2021, 20% of them received at least one mRNA dose and 3% received two doses; by March 1, 49% received at least one dose and 22% received two doses (Figure 1). The mean interval between doses was 20.8 days (standard deviation [SD]: 2.7) for those who received two BNT162b2 doses and 28.0 days (SD: 3.5) days for those who received two mRNA-1273 doses.

Most cohort members were male (96%), younger than 60 years (88%), and either Hispanic or Latino (43%) or non-Hispanic Black or African American (33%). Most had risk factors for severe outcomes from COVID-19 infection: 84% had at least one medical condition defined by CDC as a marker of severe COVID-19-related illness [6], and 31% had moderate or high COVID-19 risk according to CDCR's scoring algorithm. Cohort members who had received one or more vaccine doses by the end of the study period tended to be older than those who had not, and were more likely to have medical conditions and higher COVID-19 risk scores and be non-Hispanic White or Hispanic or Latino.

Testing rates by vaccination category

Cohort members had a median of 6 COVID-19 tests during the study period (interquartile range:

2-10). Testing rates were lower in the unvaccinated group. In January 2021, for example, there were 933 tests per 10,000 person-days among the unvaccinated group, compared with 1167 among the partially vaccinated group ($\geq$ 14 days after first dose until receipt of second dose) and 2018 among the fully vaccinated group ($\geq$ 14 days after second dose). The rate of testing decreased from 957 tests per 10,000 person-days in January to 886 in February.

Confirmed infections and other COVID-19 outcomes

A total of 13,216 confirmed infections (37.8 per 10,000 person-days), 393 hospitalizations (1.1 per 10,000 person-days), and 48 deaths (0.1 per 10,000 person-days) were documented among cohort members. Most of these outcomes occurred among unvaccinated people (Table [**?**]). Incidence of confirmed infection was 0.6 per 10,000 person-days among the fully vaccinated, 3.5 among the partially vaccinated, and 46.8 among the unvaccinated. Incidence of infection decreased during the study period, from 40.2 per 10,000 person-days in January 2021 to 11.8 in February (Figure [**?**]).

Vaccine effectiveness

There was no significant difference in the adjusted hazard ratio for confirmed SARS-CoV-2 infection during days 0 to 6 days after receiving a first dose relative to unvaccinated status (Table [**?**]). From 7 to 13 days after a first dose, estimated vaccine effectiveness was 44% (95% CI, 20-61%), and from 14 days after a first dose until receipt of a second dose, effectiveness was 74% (95% CI, 64-82%). Effectiveness estimates were 85% (95% CI, 66-94%) from 0 to 13 days after a second dose and 97% (95% CI, 88-99%) from 14 days after a second dose.

Secondary analyses

Subgroup analyses produced similar estimates of effectiveness to the full cohort analysis (Table S3A). Among those receiving the mRNA-1273 vaccine, estimated effectiveness was 71% (95% CI, 58-80%) from 14 days after first dose until receipt of second dose and 96% (95% CI, 67-99%) from 14 days after second dose. Among cohort members at moderate or high risk for severe COVID-19 illness, effectiveness estimates were 74% (95% CI, 62-82%) from 14 days after first dose until receipt of second dose and 92% (95% CI, 74-98%) from 14 days after second dose.

Estimates in an expanded cohort that included new entrants and residents with prior infections did not differ appreciably from the main cohort analysis. Results were also insensitive to model specification choices, including censoring of observation time at the date of cohort members' last test and clustering standard errors at different residential levels.

In secondary analyses that modified the study end date, effectiveness estimates for fully vaccinated residents (i.e., from 14 days after second dose) decreased from 98% (95% CI, 82-100%) to 82% (95% CI, 69-89%) over a series of end dates between February 15 and July 1, 2021. Study months spanning March to July were characterized by significantly lower outbreak risks across all facilities

COVID-19 Vaccination Status	**Confirmed Infection**	**Hospitalized**	**Died**	**Tested**	**Total**	**Median Follow-up**	**Person-Days**	**Positive per 10,000 Person-Days**	**Effectiveness, Unadjusted**	**Effectiveness, Adjusted**
Unvaccinated	12,318	356	44	53,415	60,673	43	2,633,734	46.8	(Ref)	(Ref)
Vaccinated with 1 dose										
0–6 days after first dose	527	20	3	19,767	29,947	7	206,960	25.5	–4 (–44 to 25)	16 (–15 to 39)
7–13 days after first dose	237	11	1	17,200	28,902	7	199,746	11.9	26 (–8 to 50)	44 (20–61)
$\geq$ 14 days after first dose until second dose	101	4	0	16,436	27,392	11	286,856	3.5	63 (48–74)	74 (64–82)
Vaccinated with 2 doses										
0–13 days after second dose	30	2	0	7,152	13,183	11	120,141	2.5	74 (41–89)	85 (66–94)
$\geq$ 14 days after second dose	3	0	0	2,381	3,659	14	50,033	0.6	93 (76–98)	97 (88–99)

Table 1.1: Persons, Person-Days, and Vaccine Effectiveness Against Coronavirus Disease 2019 Infection Among Study Cohort of Incarcerated People in California State Prisons, by Vaccination Status, 22 December 2020 to 1 March 2021.

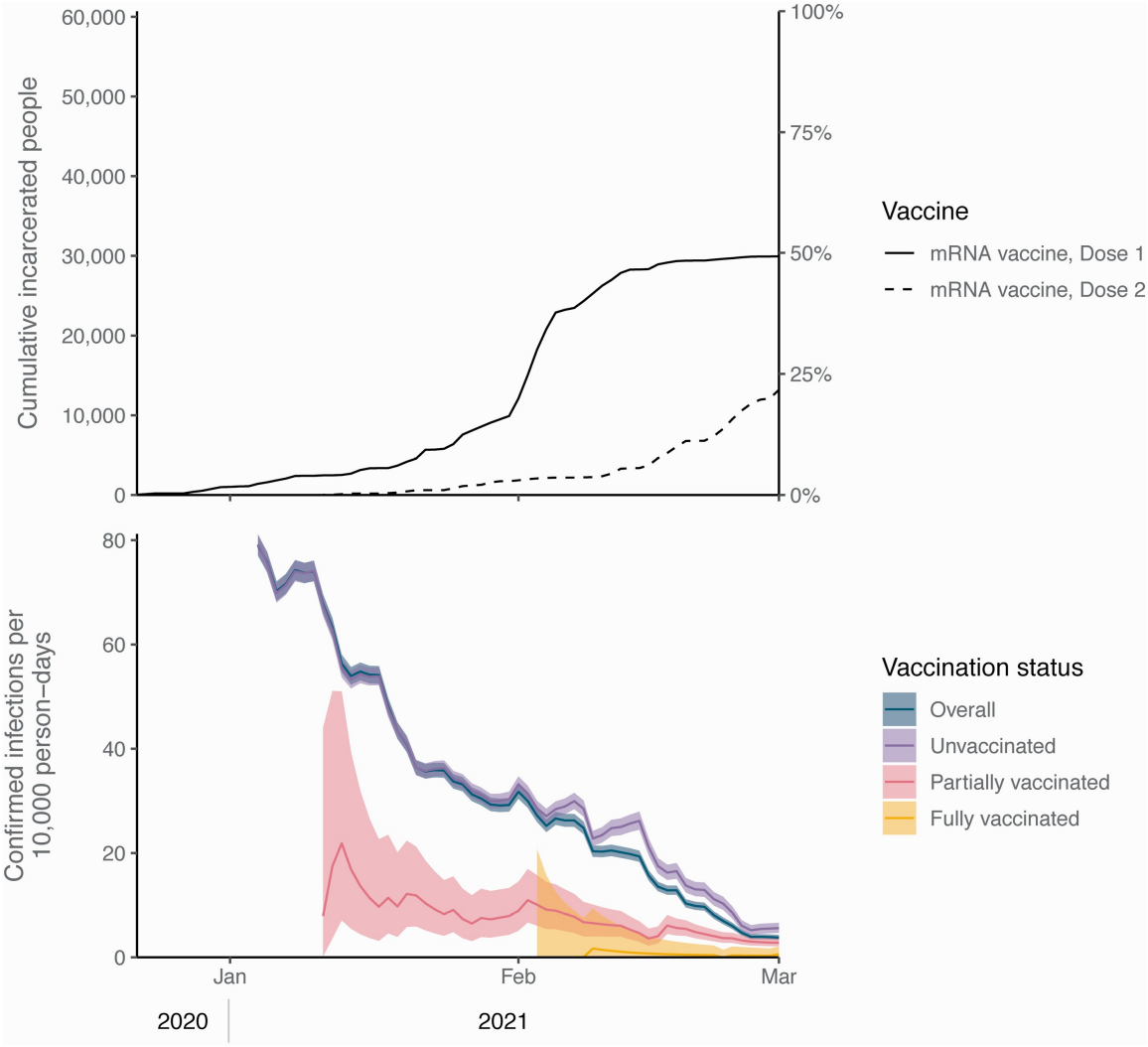


Figure 1.7: Cumulative vaccinations with 1 or 2 doses of messenger RNA (mRNA) vaccines (top panel) and 14-day rolling rates of confirmed infections per 10,000 person-days by vaccination status (bottom panel), among study cohort of incarcerated people in California state prisons without confirmed infections prior to 22 December 2020. Time periods with $<$ 200 people tested were excluded. Shaded areas represent 95% confidence intervals. Partially vaccinated status defined as geq14 days after a first dose until receipt of a second dose; fully vaccinated status defined as geq14 days after a second dose.

(0.4 confirmed infections per 10,000 person-days); lower testing (474 tests per 10,000 person-days); and high overall vaccination coverage rates (72% and 75% of cohort members who were still in custody had received at least one dose or had tested positive by April 1 and July 1, respectively).

Discussion

This study found that BNT162b2 and mRNA-1273 vaccines were highly effective against confirmed SARS-CoV-2 infection among members of a high-risk and racially diverse population of incarcerated people. Beginning 14 days after a second mRNA vaccine dose, estimated effectiveness in this population was 97%. The vaccines were also highly effective among prison residents at higher risk for severe COVID-19 illness.

Our estimates of effectiveness among fully-vaccinated people in California prisons was higher than estimates reported by Cavanaugh et al [37] from a skilled nursing facility (66% among residents and 76% among staff from 14 days after a second BNT162b2 dose), though similar to those reported for healthcare and other frontline workers by Thompson et al [119] (91% from 14 days after second mRNA vaccine dose) and Angel et al [25] (86% from 7 days after second BNT162b2 dose). Population-level studies in Israel by Dagan et al [15] and Haas et al [63] also reported similar results (92% and 95%, respectively, from 7 days after second BNT162b2 dose) as our study. Estimates of effectiveness of partial vaccination are more variable. We estimated 74% effectiveness against infection from 14 days after a first mRNA vaccine dose until receipt of second dose. This result was lower than Thompson et al's [119] estimate of 81% among healthcare and other frontline workers from 14 days after first mRNA vaccine dose until 14 days after second dose, but substantially higher than Dagan et al's [15] estimates of 46% for days 14 through 20 after first BNT162b2 dose and 60% for days 21 through 27.

To our knowledge, this is the first study to assess effectiveness of a COVID-19 vaccination program in a carceral setting. It has several strengths. We used detailed daily information on vaccination status and key COVID-19 outcomes for each resident. These data allowed us to adjust for key potential confounders, including risk factors for severe COVID-19, housing arrangements, and participation in penal labor. An extensive testing program in this population facilitated relatively complete measurement of SARS-CoV-2 infections. In addition, the large sample size permitted estimates of effectiveness within particular subgroups of interest (e.g., medically vulnerable).

Understanding vaccine effectiveness among people at high risk for severe disease is a priority. Our estimated effectiveness for partial and full vaccination did not differ appreciably between the full cohort and subsets characterized by moderate or high risk for severe COVID-19 illness. This bolsters growing evidence that mRNA vaccines provide substantial protection in older adults [117, 15], people with pre-existing conditions [15, 122], and residents of skilled nursing facilities [37, 34]. Our results also extend evidence from studies of healthcare workers indicating these vaccines are effective in environments characterized by high transmission risks.

In observational cohort studies like ours, potential for bias due to confounding is an important consideration. Vaccines were not offered randomly to residents—in particular those with risk factors for severe disease were prioritized. Given the latency of biologically plausible protection, the days after vaccination can serve as an indicator of bias, with large effectiveness estimates signaling substantial residual confounding [72]. We included an exposure category for the first week after a first mRNA vaccine dose to assess the presence of such residual confounding, and detected a statistically insignificant 16% effectiveness for this negative control exposure. Vasileiou et al [122]. reported a much higher estimate, 86% protection against COVID-19 hospitalizations during the first week after vaccination for BNT162b2, in a previous study on effectiveness in Scotland.

Residents were tested frequently (median 6 tests) during the 70-day study period, but testing was neither routine, random nor compulsory, creating potential for ascertainment bias. Several results provide some reassurance in this regard. First, vaccinated cohort members overall had 25% higher testing rates than unvaccinated members. Thus, the most plausible bias from differential testing would be more complete case detection among the vaccinated, which would lead to underestimating vaccine effectiveness. Second, an analysis that censored follow-up on the last test collection date for a cohort member produced effectiveness estimates similar to those from the main analysis.

Extending the study period through July 1, 2021 added four months in which testing and case rates were low, and a relatively large proportion of prison residents had been vaccinated. We found lower levels of estimated effectiveness for the fully vaccinated group over this extended period—an expected result, and a trend seen in the six-month vaccine efficacy clinical trial for the BNT162b2 vaccine [118]. Accumulation of undetected infections that confer natural immunity may have contributed to dilution of estimated effectiveness, especially among residents at lower risk for severe COVID-19, who were generally tested less frequently and vaccinated later in the study period. Additional contributors may have included increasing bias in the composition of the unvaccinated group towards residents who declined vaccination, as well as cohort selection induced by heterogeneity in infection risk [60]. For instance, if the vaccine offered partial (or "leaky") protection [87], high infection risk within an unvaccinated group that is initially highly susceptible could induce selection bias over time as the most susceptible people are removed from the group, which would decrease estimated effectiveness of vaccination.

The study has several other limitations. First, our estimates of effectiveness focused on confirmed infections, not other important outcomes, such as symptomatic infections or severe disease. Incidence of hospitalizations and deaths in our cohort during the study period was too low to support rigorous analysis of those outcomes, and symptom reporting is unreliable in carceral settings [107]. A related point is that we were only able to estimate effectiveness in relation to the date of test sample collection, not transmission date, which allows for the possibility that some detected infections might have preceded vaccination. Second, we evaluated effectiveness against any SARS-CoV-2 infection, not specific viral variants, because CDCR conducted limited viral genome sequencing during the

study period. As the B.1.617.2 (delta) variant became dominant and cases rose in the general community over the months of June and July [19, 16], CDCR detected a total of 286 cases among a population of nearly 99,000 residents during this period [17], a substantially lower rate when compared to the period between mid-March 2020 to mid-February 2021, during which the number of cases were above 200 in almost every week, peaking at 5659 weekly cases in December 2020. Low incidence after February 2021 suggests that there may be substantial protection against outbreaks in this population with high levels of vaccination and prior infections, including during a period marked by increasing prevalence of more highly transmissible variants. However, as people continue to become infected and more outbreaks occur, further follow-up is necessary to reassess the effectiveness and protection afforded by vaccines. Third, CDCR used some antigen tests, which have lower sensitivity, potentially leading to under-detection of cases. However, at least 93% of all tests were PCR, so we expect any bias related to antigen testing to be minimal. Finally, the generalizability of our results to residents of jails and other correctional systems is unknown.

Residents of prisons and jails have borne a disproportionately large share of disease burden during the COVID-19 pandemic. Findings from this study–building on a growing evidence base indicating vaccine efficacy and effectiveness across a range of populations and settings–suggest that mRNA vaccines are extremely effective in protecting incarcerated people against infection, including residents at high risk of severe COVID-19 illness. Continued emphasis on vaccination and other ongoing mitigation practices are essential in preventing COVID-19 in this disproportionately affected population. Incarcerated people, correctional workers, and the wider community all stand to benefit from those efforts.

Chapter 2

Equity in social policies

2.1 Background

An open-source data tool is used in California to identify "disadvantaged communities" considered most vulnerable to environmental exposures, a designation through which hundreds of millions of dollars in social welfare funding is allocated annually. Due to the lack of ground truth in determining disadvantaged communities, creating a single index to determine environmental vulnerability is inevitably a subjective task. We audit the data tool and compare it with plausible model alternatives, finding technical errors, measurement errors, and subjective model choices that ultimately lead to substantial variations in funding allocations. We urge that tools such as this should be designed by and in collaboration with community leaders, domain experts, and regulatory agencies in order to avert misallocation of funding and exacerbation of social inequities.

In 2012, California Senate Bill 535 was signed into law, allocating 25% of California's proceeds from its cap-and-trade program to social welfare funds for environmentally disadvantaged communities. CalEnviroScreen, an open-source data tool, was created by CalEPA to identify and designate disadvantaged communities. The tool directs about $200 million of funding annually from California's cap-and-trade program alone; it also directly influences funding from a variety of public and private sources, and is reported to have directed an estimated $12.7 billion in funding.

The tool takes Census tract-level data on pollution burden and population characteristics and reduces it into a single score; the Census tracts in the top 25% of scores are designated "disadvantaged communities." The pollution burden category is split into two subcategories: exposures and environmental effects; the population characteristics category is also split into two subcategories: socioeconomic factors and sensitive populations. All categories are weighted equally except for environmental effects, which is half-weighted. Variables in each subcategory are converted to ranked percentiles then averaged together into a subcategory score. The subcategory scores are then averaged into category scores (pollution burden and population characteristics), which are

then multiplied together to create a CalEnviroScreen (CES) score (Figure 2.1).

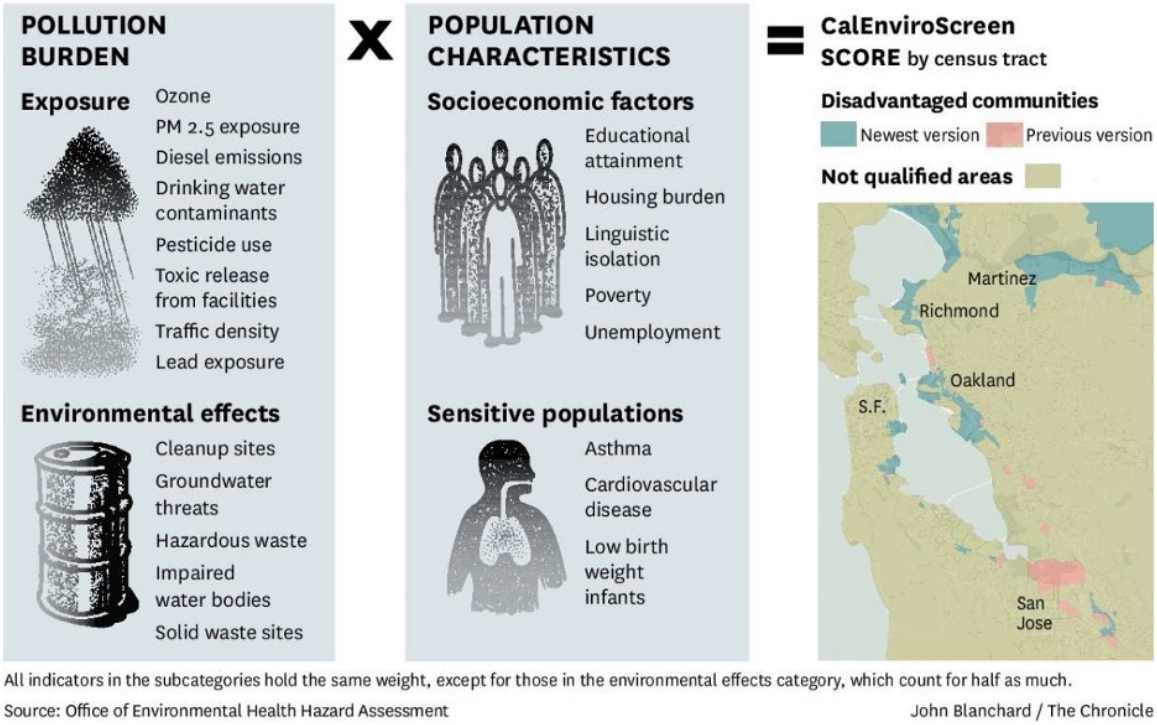


Figure 2.1: Calculating the CalEnviroScreen Score. CalEnviroScreen is a formula that balances dozens of factors to determine the state's most vulnerable commmunities, labeling the top quartile of census tracts as "disadvantaged." The designation is used to prioritize communities for billions of dollars in government and private funding.

2.2 Methods

Prior to data analysis, we identified potential flaws in the data tool and conceived plausible alternative models. We then built the alternative models and evaluated how they differed from the original model.

2.2.1 Subjectivity in pre-processing

We propose using Z-score standardization instead of percentile ranking as a way of converting each variable onto the same scale before converting into an index. Percentile ranking changes the distribution of each variable into a uniform distribution and is not typically used as a scaling procedure; Z-score standardization preserves the original distribution of the raw data and is widely used as a scaling procedure.

Additionally, we propose averaging the pollution burden and population characteristics together to create the CES score instead of multiplying them. Multiplying the two category scores inflates high values and deflates low values from the category scores, exacerbating existing model error.

2.2.2 Measurement error

Currently, the data tool uses emergency room visits for asthma and myocardial infarction as proxies for respiratory and cardiovascular health, respectively. Using ER visits as a metric is potentially biased: although on average, lower-income populations use the ER disproportionately more, some subgroups, such as immigrant populations, use the ER disproportionately less. We propose using a mix of ER visits and Census tract-level survey data for a more robust estimate of respiratory and cardiovascular health.

2.2.3 Model design

The inclusion and exclusion of variables to use in the model is inherently a subjective choice and can result in inadvertent model bias. For example, we identify the use of asthma as a representative of respiratory health as a potentially biased indicator. Because asthma is less prevalent in developing countries, it is disproportionately less prevalent amongst immigrant populations in the US; consequently, the model is potentially biased against neighborhoods with large immigrant populations. As an alternative, we propose using a mix of asthma and chronic obstructive pulmonary disease (COPD) as an indicator for respiratory health.

Additionally, respiratory and cardiovascular health are not the only areas of health affected by environmental exposures. We propose using more indicators, such as renal function and neurological disorders.

2.2.4 Evaluation

We evaluate model agreement between the original model and alternative models using a variety of metrics ranging from area under the ROC curve, precision-recall, Cohen's Kappa, etc. We also evaluate heterogeneity in model agreement using discordance as a metric: if discordance between two models increases as a protected attribute (e.g., race, age, etc) also increases, then the difference in models presents as bias against the protected attribute.

2.3 Results

2.3.1 Subjectivity in pre-processing

Percentile pre-processing greatly distorts the distribution of variables. For example, general scientific literature suggests that PM2.5 is linearly related with health outcomes. However, the difference between the 80th to 90th percentiles is just $0.3\mu g/m^3$ whereas the difference between the 90th to 100th percentiles is $4.1\mu g/m^3$ (Figure 2.2

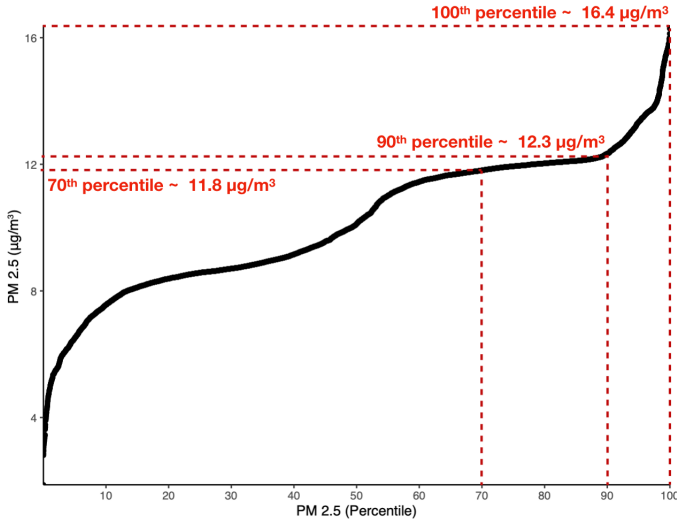


Figure 2.2: Percentile versus raw PM2.5 distribution.

While the model agreement across the state was quite high, at 0.91, this small change in pre-processing is disproportionately large for certain geographic regions. In San Francisco, census tracts classified as disadvantaged were quite varied between pre-processing techniques (Figure **??**). The reason for this is two-fold. Percentile ranking is extremely sensitive, especially in the presence of measurement error. Perhaps a larger issue is one that pertains to fair allocation to cities. Percentile ranking artificially deflates the impact measurements where a census tract is an outlier. This is especially consequential for cities such as San Francisco where the city may regulate most pollution burdens such as pesticides, solid waste, cleanup sites, ozone, and PM2.5, but that there are census tracts within the city that are outliers for other measures.

2.3.2 Measurement error

Measuring incidence of disease is highly variable, especially for spatially granular units such as census tracts. Health estimates used in CalEnviroScreen are estimated using emergency room visits. The Centers for Disease Control and Prevention also release census tract-level estimates, which uses a

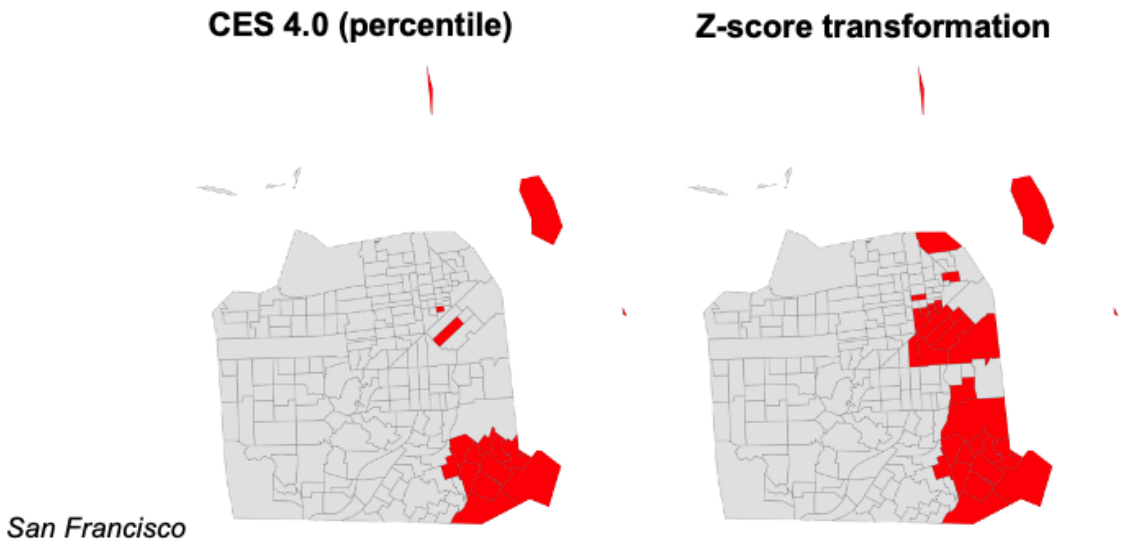


Figure 2.3: Disadvantaged census tracts in San Francisco classified under percentile versus Z-score pre-processing.

modeling approach to extrapolate from health surveys. The correlation between these two databases are low (Figure 2.4), with asthma having an R^2 of 0.31 and cardiovascular disease having an R^2 of 0.05.

Health metrics are very difficult to measurement and prone to bias, especially at this level of granularity. Census tracts give a false sense of precision, despite the levels of measurement error. Additionally, each method of measurement is prone to their own source of bias. For example, ER-based measures may underestimate the prevalence of disease for subgroups that may underutilize ERs.

2.3.3 Model design

Air pollution is known to cause and exacerbate a variety of respiratory diseases such as asthma and Chronic obstructive pulmonary disease otherwise known as COPD. Under the current algorithm, asthma is the only respiratory disease that is included.

However, auditing fairness for this algorithm is challenging. First, it is an unsupervised settings, so unlike many other fairness applications, there is no ground truth. Second, the unit of observation is census tracts, which are aggregate population units with continuous attributes of race, immigration history, and socioeconomic status, so traditional evaluation metrics such as group fairness will not work.

To apply fairness to unsupervised settings, we propose using discordance between two models as a metric of change between a proposed model and the current model. Additionally, to examine fairness

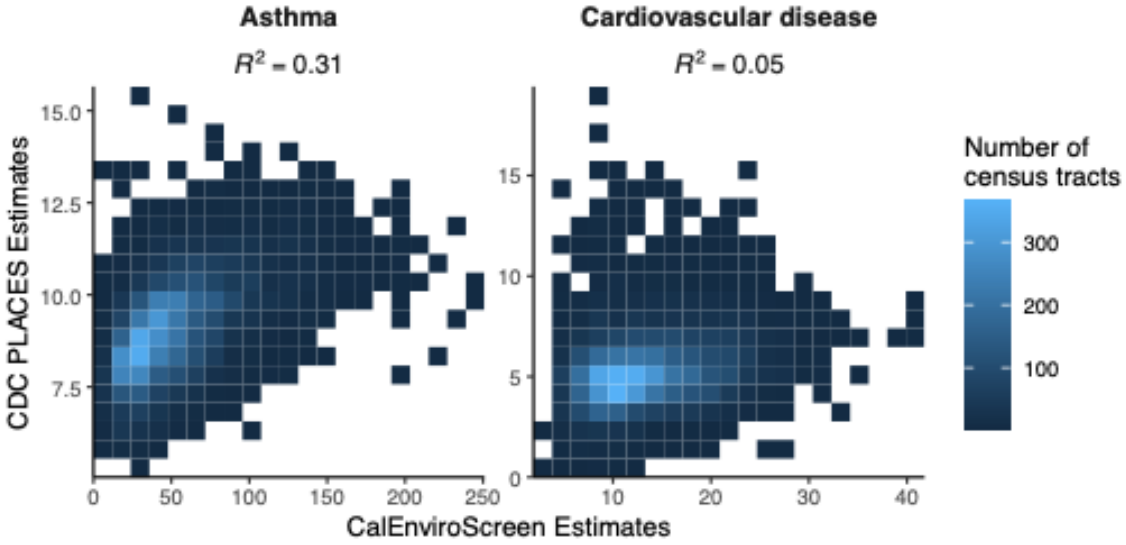


Figure 2.4: Density plots of health metrics estimated from surveys and ER visits.

over continuous, we propose examining the relationship between discordance and the continuous attribute. To test the hypothesis that asthma may be a potentially biased indicator of respiratory health, we compare census tracts designated as disadvantaged under the current algorithm and the model with COPD instead of asthma. We calculate the pairwise discordance of disadvantage status between the two models by the percent foreign born of each census tract (Figure **??**). A positive discordance indicates that a census tract was more likely to be designated as disadvantaged in the COPD model compared to the asthma model.

As census tracts increase in percent foreign born, discordance increases. Given that California is a state with a large immigrant population, this subjective choice may lead to under-funding within immigrant populations.

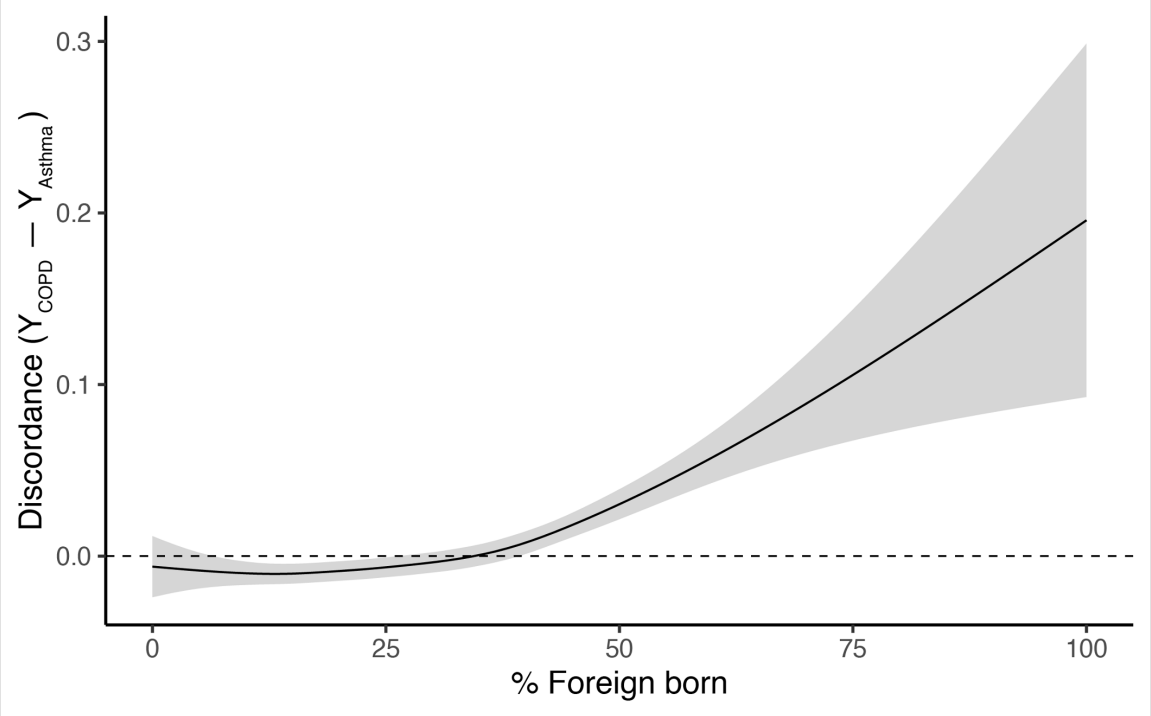


Figure 2.5: Discordance between asthma and chronic inflammatory lung disease models.

Chapter 3

Methods in precision health

3.1 Gene network rewiring in heart failure

3.1.1 Introduction

Heart failure (HF) is a life-threatening syndrome characterized by an inability of the heart to meet the metabolic demands of the body. HF costs the US more than $34 billion a year to treat 6 million patients[79, 52]. Despite this, the underlying molecular mechanisms remain poorly understood and the few approved therapeutics target maladaptive compensatory pathology rather than proximate molecular mechanisms[111, 97].

With rapidly increasing access to high throughput sequencing technology, molecular characterization of human heart tissue has become possible, and in recent years a number of efforts to define the regulatory transcriptional architecture of HF in humans and small animals have been undertaken [39, 81, 67, 121, 66, 64, 70, 94]. These efforts have revealed changes in gene expression of key sarcomeric, calcium cycling, developmental and metabolic genes. Because of the significant logistical challenge of harvesting healthy hearts, few studies have included a non-failing control group, making conclusions regarding the transition to HF tentative. Further, as gene expression programs are rapidly altered in an environment of high oxidative and nitrosative stress [93], the high metabolic rate of the heart limits the utility of post-mortem tissue for gene expression analysis (e.g., from public resources such as GTEx [61, 88, 62]).

Thus, the expansion of this resource with high fidelity tissue collection and molecular characterization is required, and a crucial next step in synthesizing this information is the identification, and in vitro and in vivo validation, of novel molecular actors in this disease. In this study, we identify previously undetected cardiac expression quantitative trait loci (eQTLS) from genome-wide genotyping and gene expression measurements from rapidly preserved failing and non-failing human heart tissue.

Condition-specific cardiac regulatory gene networks identify disease-driven changes in local and global topology, illuminating PPP1R3A as a novel predicted HF regulator. Lastly, our in vitro and in vivo approaches further demonstrate its role in HF pathology.

3.1.2 Methods

Tissue collection and processing

We established a collaborative multi-institution network with a 24/7 notification system and a team of travel-ready surgeons at major transplant centers to systematize the collection of cardiac tissue from failing hearts and unused heart transplant donors at operating rooms and remote locations. We put in place a series of best practices for procurement of explanted cardiac transplant tissue including harvesting explanted cardiac tissue at the time of cardiac surgery from subjects with HF undergoing transplantation and from unused donor hearts. Hearts were perfused with cold cardioplegia solution prior to cardiectomy to arrest contraction and prevent ischemic damage, and explanted cardiac tissue specimens were flash frozen in liquid nitrogen.

All samples were taken from the left ventricular free wall at the mid ventricular level (Segments 11 or 12) on the 17-segment model. On some of occasions, when it was necessary to avoid infarct or peri-infarct tissue in these segments, we obtained tissues that may be closer to the base or apex or more anterior or inferior (segments 1, 4, 5, 6, 7, 10, 16). The septum was never collected. Histopathology using H&E and trichrome staining were used to avoid the use of donor hearts with excess fibrosis or hypertrophy. Immunostaining was not performed.

The institutional review boards at all collection sites (including Stanford, the University of Pennsylvania and the Cleveland Clinic) reviewed and approved the protocols used in this study for procurement and use of human tissue and information. All participants gave informed consent before enrollment.

Expression and genotype datasets and clinical variables

We performed RNA expression measurements and obtained genotype information in genome-wide markers for 313 patients (177 failing hearts, 136 donor, non-failing [control] hearts) using Affymetrix expression and Affymetrix Human 6.0 respectively. Clinical variables for each individual were recorded during the course of the research and were compiled using REDCap[68].

Data pre-processing, covariate correction, and differential expression

Several technical and sample covariates can bias gene expression values inferred from our microarray data, such as array batch effects and individual ethnicity, gender. These covariates can greatly confound downstream analyses, resulting in false positive and negative associations and reducing the power of statistical analyses. We corrected for these biases in three ways: by normalizing to

"reference" probes (control probes with a fixed fluorescence value that control for the geometry and preparation of the array), by applying batch normalization using ComBat[120], and by correcting for observed covariates (gender, age, and collection site) using robust linear regression. The residuals after these corrections were then used as the gene expression values for downstream analyses. Previously to these corrections, the data was log-transformed to better resemble a normal distribution. Differential expression analysis was performed using the Significance Analysis of Microarrays (SAM) [110]. Genes shown in Figure 3.1B had the highest gene expression difference and were deemed significantly up or down regulated with a false discovery rate of 5%. QQ plots for differential expression are shown in Figure 3.2.

Co-expression networks

We ran the following methods on the covariate-corrected data described in the section above using the top 40% most variable genes (n=7960) and on each cohort separately, except in the case of the joint graphical LASSO (see below).

- WGCNA: We ran the WGCNA pipeline including correlation matrix, TOM transformation, and Dynamic Tree Cut module finding as prescribed 19 on each network separately.
- Pearson correlation: We obtained the empirical Pearson correlation matrix and performed an absolute correlation coefficient cutoff of $abs(R) > 0.6$.
- ARACNe: We ran the method with default parameters and 500 bootstrap iterations for calculating significant gene co-expression relationships.
- Z-score: Otherwise known as the CLR method, we ran the method using the Pearson correlation matrix as input. The output is then a statistical scoring of each interaction for genes A and B considering all interactions of A and B against each other gene.
- Joint graphical LASSO (JGL): The JGL has two main parameters – a sparsity penalty to tune how many interactions are found and a group penalty that tries to match the network structure of the two cohorts. We performed a grid search on these parameters and chose the one that maximized the Akaike Information Criterion. This resulted in a very low group penalty of 0.01 and a modicum sparsity penalty of 0.1, which was applied to a standardized matrix of expression values for both cohorts.

eQTL discovery

Prior to eQTL discovery, we used PEER to find hidden covariates that could confound signals in our data as well as filtering any genotypes with major allele frequencies less than 5%. To test associations between gene expression in each cohort separately, we used QTLTools[48] with an additive model

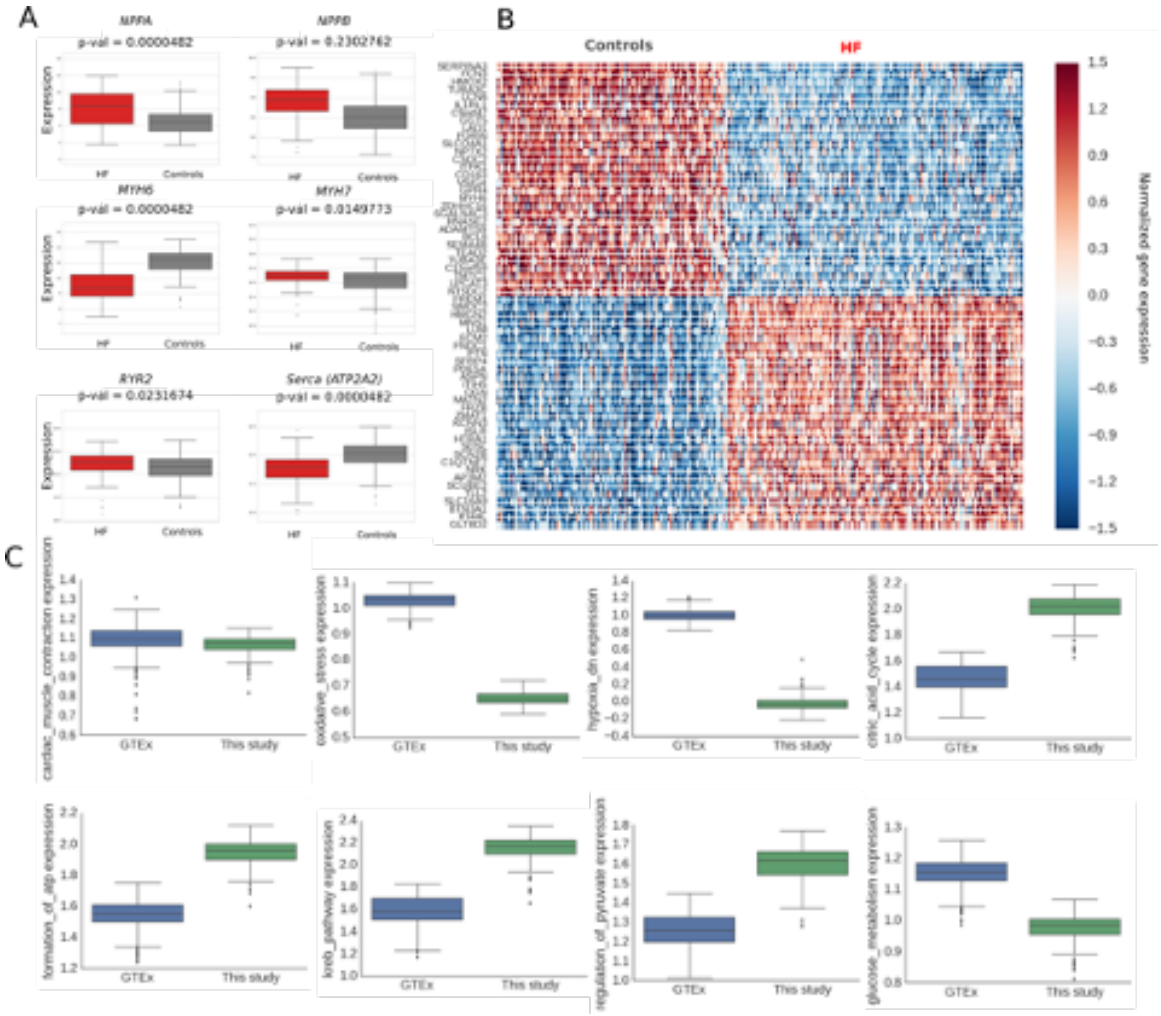


Figure 3.1: (A) Expression of various genes involved in heart failure in the failing and non-failing control cohorts. (P-values as indicated). (B) Top differentially expressed genes between failing and non-failing controls.(C) Mean expression of various gene sets, including metabolic pathways and oxidative stress/hypoxia genes of the GTEx post-mortem samples (blue) and the control cohort in this study (green) obtained from heart transplant donor hearts. Error bars indicate one standard deviation.

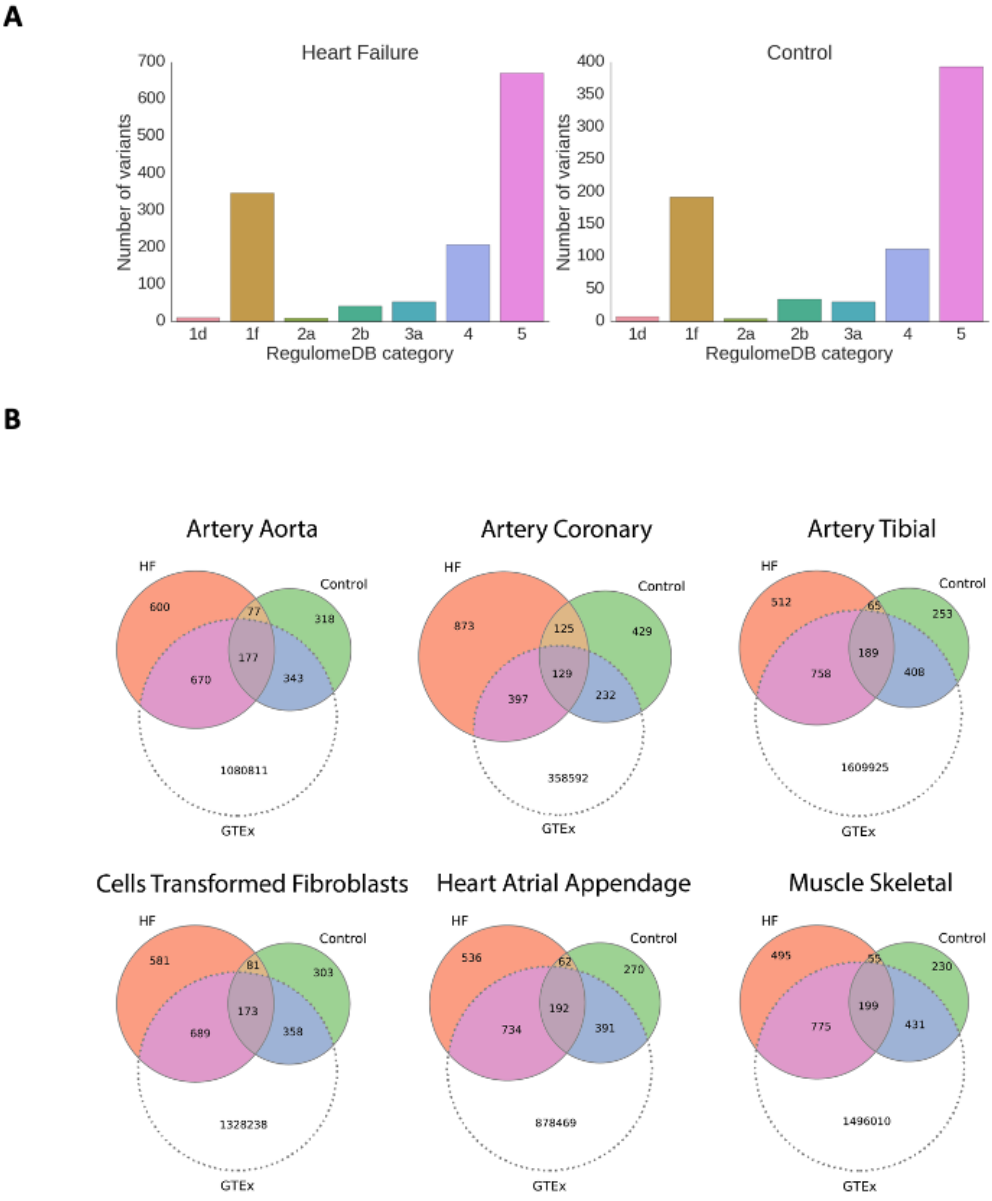


Figure 3.2: (A) Number of eQTLs for each network for which there were RegulomeDB annotations within a 50 base pair window. RegulomeDB categories are defined as follows: category 1 are known eQTLs with ENCODE DNase sensitivity peaks (1f) and TF binding data (1d); category 2 only have evidence of TF binding (2b) and DNase sensitivity peaks as well as a matching TF binding motif (2a); category 3a have predicted TF binding and a TF motif as well as DNase peak; category 4 have predicted TF binding and a DNase peak; and category 5 have either predicted TF binding or a DNase peak. (B) Venn diagrams illustrating overlap of HF and Control network eQTLs by relevant tissue type in GTEX.

accounting for gender, age, sample site, and the PEER factors as covariates. We corrected for eQTL multiple association testing using a 10000 permutations per locus in a 2 megabase window and a false discovery rate cutoff of 5%. To select the number of PEER factors, we performed the full analysis multiple times from 1 to 15 PEER factors and observed a saturation of new QTLs being discovered when using 10 factors. To intersect our variants with GTEX and the GWAS catalog, we simply matched based on rsid and position. High-resolution co-localization analysis on coronary artery disease GWAS hits was performed using the eCAVIAR pipeline (see details in Methods) [31]. To find independent eQTLs, we performed LD-pruning (LD, pairwise r $2 < 0.5$ within a window of 50 kb). QQ plots for eQTL p-values before and after correction for age, gender and site are provided in Figure 3.3, and were not significantly inflated by batch correction.

Cardiac GWAS co-localization analysis

We tested whether any of our eQTLs co-localized with the signals from a publicly available GWAS on coronary artery disease54. We ran the eCAVIAR [74] pipeline using the FINEMAP implementation on all loci with at least one SNP with $p < 1e-5$ in the GWAS and at least one SNP with $p < 1e-5$ in either condition of our eQTL study. We found evidence of co-localization at 6 genes: MRAS, TCF21, GPR22, LIPA, ZNF664, and EIF2B2. EIF2B2, TCF21, and ZNF664 co-localized in both failing and healthy hearts. However, LIPA co-localized only in healthy hearts, while GPR22 and MRAS co-localized only in failing hearts. These context-specific co-localizations highlight genes that may contribute to heart disease progression specifically in healthy (LIPA) or in already-failing hearts (GPR22, MRAS). LIPA codes for the lysosomal enzyme lipase A. GPR22 has previously been shown to play a protective role against myocardial stress[**?**]. The protein MRAS is a muscle-expressed homolog of the Ras oncogene family, currently without any well-characterized mechanism in coronary artery disease.

Quantifying global and local centrality using network and community membership parameters

The local connectivity metric (LC) of any gene G was calculated as the difference between max-normalized weighted network degree of G. The global connectivity metric (GC) of any gene G was calculated as the number of gene sets that were significantly differentially enriched between gene rankings of failing and control networks obtained by ordering the genes by their absolute correlation coefficient to G.

After inferring the gene co-expression networks for both cohorts, we calculated topological properties for each gene in each network in order to get a sense of a gene's role in the networks and in the context of known pathways and gene sets. To this end, we defined a gene g's differential global connectivity (GC) as the number of curated HF relevant pathways within its neighborhood (defined by genes lying within a set rank of absolute edge weight to gene g) that were significantly enriched

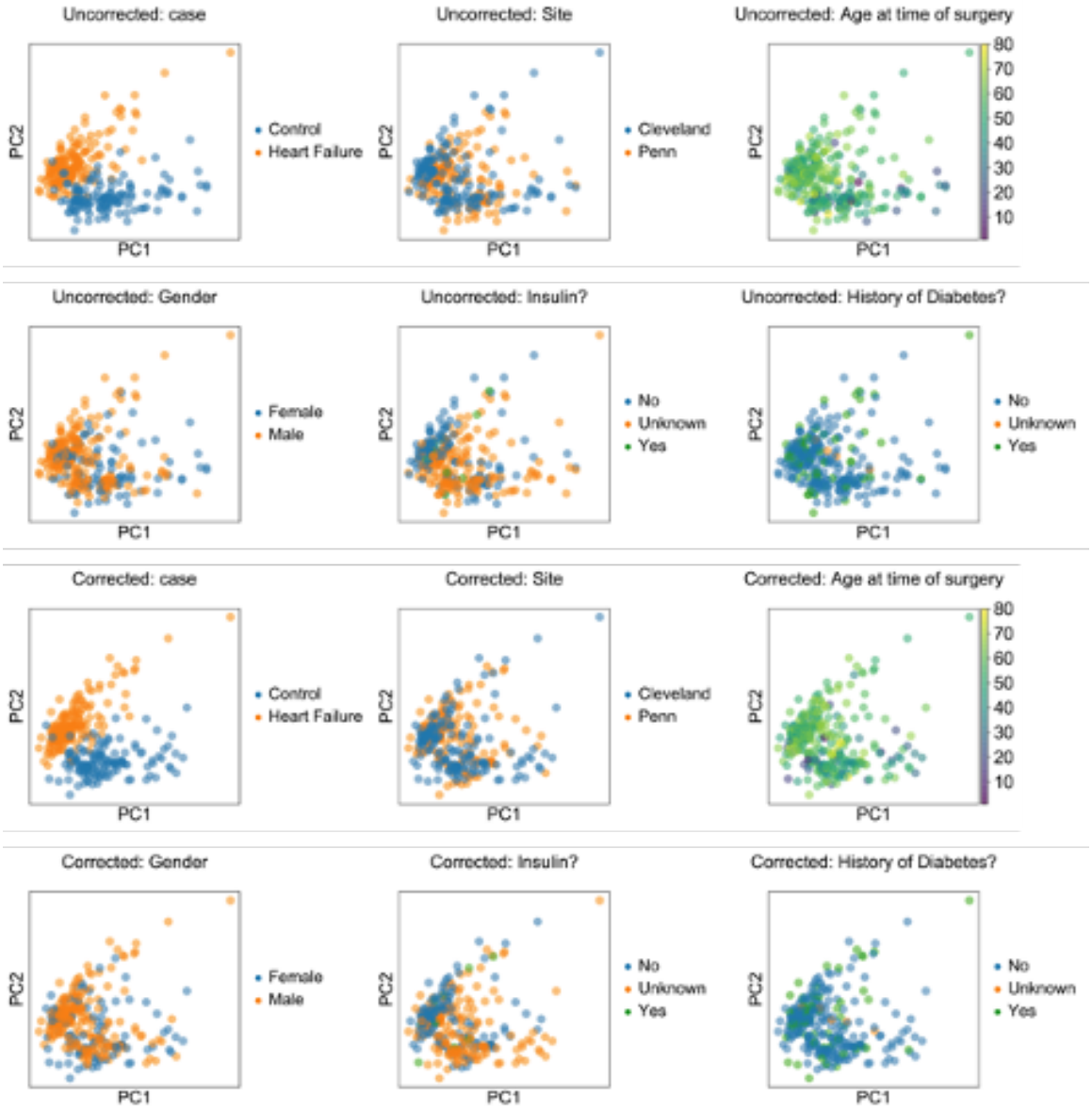


Figure 3.3: Principal Component Analysis showing lack of segregation of potential clinical confounders with components of gene expression. Patients are labeled using covariates and comorbidities plotted before and after batch correction on the first two principal components.

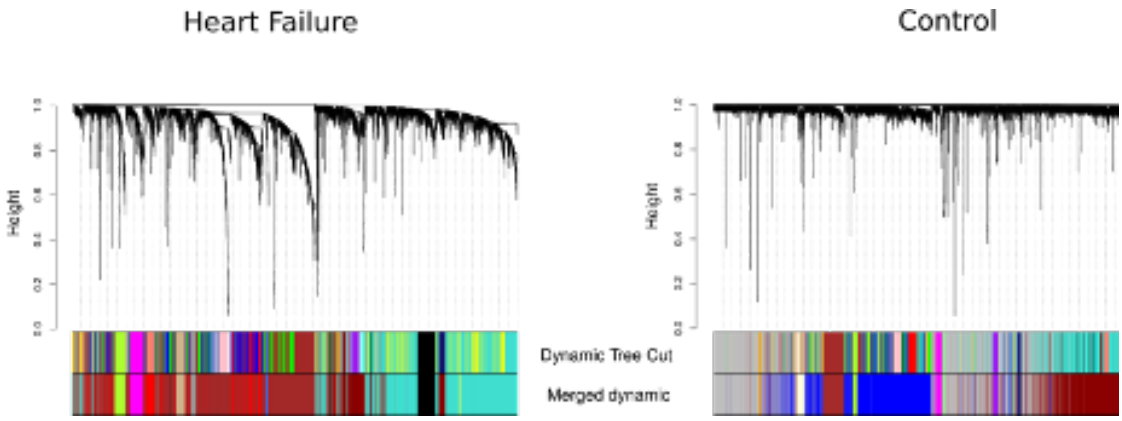


Figure 3.4: Dendrograms from WGCNA HF (left) and control (right) networks. While the number of modules found in each network are similar (12 for HF and 13 for controls), dendrograms visually indicate a more cohesive structure in HF compared to controls, with 2614 genes unassigned to any module in the control (gray module) compared to only 13 in HF.

in g's neighborhood by the following procedure (see Figure 3.4):

1. For each pathway, we first ranked the neighbors of g by their absolute edge weight (i.e. correlation) to g in both the HF and control networks. This resulted into two ranked lists of g's neighbors: HF- and control-network specific.

2. For each gene g, we plotted the number of network neighbors belonging to a curated list of known HF-relevant pathways from KEGG and Reactome. In this analysis, the number of HF-relevant neighbors of gene g in each pathway was plotted on the y axis against progressively larger inclusive neighborhoods. This allowed us to create a distribution of global-HF pathway relatedness taking both known HF-relevant neighbors as well as their distance from gene g into account. For example, as shown for MYH7, MYBPC3, and PPP1R3A for the KEGG HCM pathway in Figure 3.5 D-E, there is a steeper rise in the number of HF-relevant neighbors connected to each gene in the HF network than in the control network.

3. For each gene g in each pathway, the difference between the HF network and control network curves was evaluated using the Kolmogorov-Smirnov (KS) statistic (analogous to gene set enrichment analysis 56) with a Benjamini-Hochberg correction (false discovery rate FDR=0.01).

4. A gene's GC was then defined as the number of HF-relevant pathways found to be significantly enriched in such manner.

To compare per-gene perturbations in local connectivity between HF and control networks, we defined the change in local connectivity metric LC for a gene g used for this purpose was calculated as follows: $LC(g) = deg_{norm}(g, HF_{net}) - deg_{norm}(g, Control_{net})$

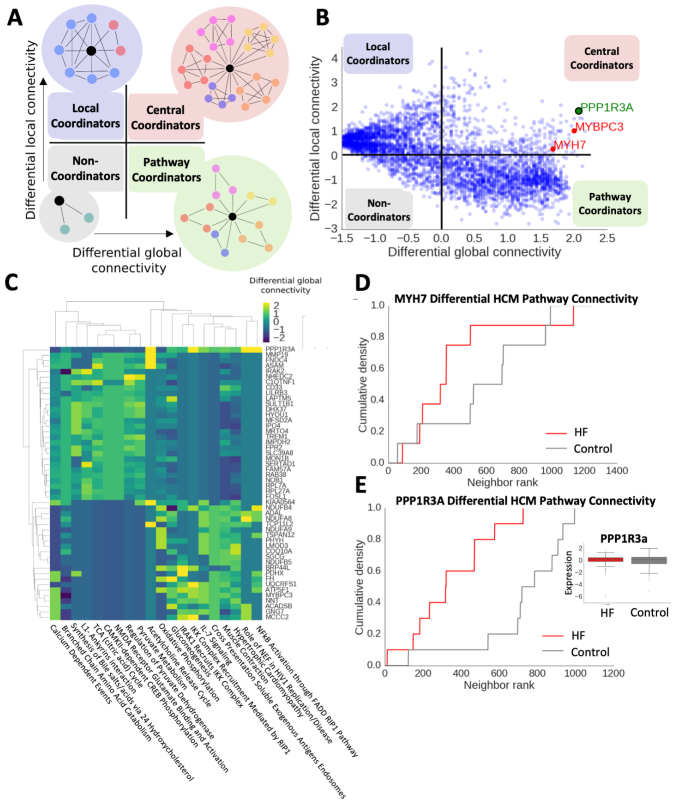


Figure 3.5: (A) Diagrammatic representation of roles of local and global connectivity in defining each gene's coordinator status. Local connectivity (LC) is the per-gene change in co-expression edges in the HF versus control network. Global connectivity (GC) represents the enrichment of HF-relevant pathways in a gene's neighborhood between HF and control networks (see Methods). (B) Change in local and global connectivity for all genes between control and HF networks identified PPP1R3A (green font) as a central coordinator in HF, indicating its increased association with HF-relevant pathways as well as co-expression relationships in the HF versus control networks. (C) Gene-pathway (rows-columns) differential connectivity matrix for genes ranked highest for global network connectivity that is differentially increased between non-heart-failure and heart-failure conditions. Differential connectivity is measured by the KS statistic between the distribution of ranks for pathway genes in HF and non-heart-failure conditions. In particular metabolism, HF and cardiomyopathy pathways (yellow indicates an increase in connectivity to the given pathway (columns) in HF compared to control samples). (D) Difference in cumulative membership distributions for the KEGG Hypertrophic Cardiomyopathy (HCM) pathway for the myosin gene MYH7 which is known to be involved in HCM. (E) Difference for HCM pathway enrichment in the protein phosphatase 1 regulatory subunit PPP1R3A is more dramatic than for MYH7. Inset: PPP1R3A transcriptional expression in HF and Control cohorts is unchanged.

Where $deg_{norm}(g, net)$ is the max-normalized weighted degree of gene g in network net (sum of weights of edges that include g divided by the maximum network weight across all edges).

Both LC and GC are then Z-score normalized in order to call coordinator status:

- Central Coordinators have Z-score normalized LC and GC greater than zero.
- Local Coordinators have Z-score normalized LC greater than zero but GC less than zero.
- Pathway Coordinators have Z-score normalized GC greater than zero but LC less than zero.
- Non-coordinators have neither Z-score normalized GC or LC greater than zero.

RNA sequencing and analysis pipeline

After RNA extraction, RNA integrity was checked using a 2100 BioAnalyzer (Agilent); all RNA samples had an RIN of 7.0 or higher. Samples were screened for PPP1R3A knockdown efficiency and phenylephrine treatment using qRT-PCR prior to library construction. RNAseq libraries were prepared using the TrueSeq Stranded mRNA kit (Illumina), according to manufacturer instruction. Libraries were barcoded, quality-checked using a 2100 BioAnalyzer and run in rapid run flow cells in a HiSeq 2500 (Illumina), producing at least 30 million paired-end reads.

Sequencing reads were aligned to the Rattus Norvegicus rn5 UCSC reference genome using the STAR aligner [50]. Quantification and differential expression analysis of RNAseq data was performed using the Cufflinks package [120]: full transcriptome assembly was performed with Cufflinks, quantified with Cuffquant, and analyzed for differential expression using Cuffdiff. All genes deemed to be significantly up or down-regulated in the main text were called as differentially expressed by Cuffdiff.

3.1.3 Results

Immediate tissue processing yields quality transcriptomic data

The MAGnet consortium was founded to establish best practices for the harvesting of human cardiac tissue (see Methods) and to explore the genetic landscape of cardiac gene expression [67, 93, 35]. Using this consensus protocol, we obtained 1352 human cardiac samples and chose a subset of 313 hearts, including 177 failing hearts collected immediately post-transplantation and 136 healthy donor controls that were suitable for transplantation but did not reach a recipient due to logistical reasons. We genotyped and measured left-ventricular genome-wide gene expression of these samples, controlling for known covariates, specifically age, gender and collection site. Principal component analysis showed that additional exposures do not explain a significant proportion of variance in gene expression (Figures 3.6A and 3.3).

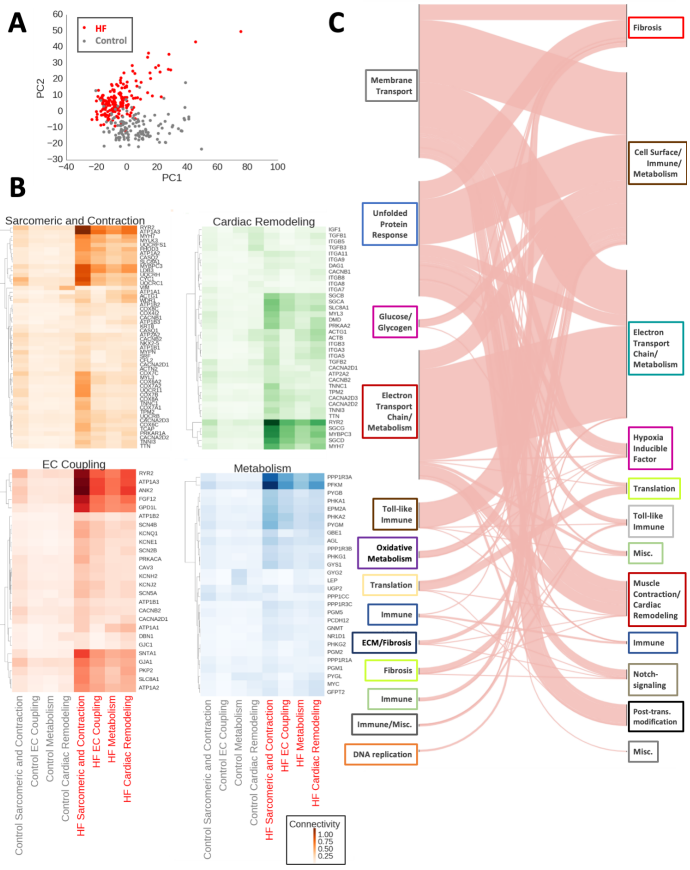


Figure 3.6: (A) Principal component analysis of gene expression profiles for 177 failing hearts and 136 non-failing, control, hearts showing clear segregation of HF (red) versus control (grey) population. (B) Differential connectivity of known biological processes in HF. Normalized connectivity (sum of WGCNA weights divided by maximum network weight) between representative genes from four known processes that play critical roles in HF (sarcomeric and contraction genes (orange), EC coupling (red), cardiac remodeling (green), and metabolism (blue)) to all genes from those same processes in HF and controls. Genes of each process are rows and columns are process and cohort. For example, MYBPC3 in the cardiac remodeling process (third row in green heat map) is highly connected to sarcomeric and contraction genes and cardiac remodeling genes in the HF network (5th and 8th columns respectively) compared to all the control processes. (C) River plot demonstrating changing modular assignments for genes in the HF vs control networks. Pink lines represent individual genes, with left sided grouping representing membership in control (left) and HF (right) network modules (indicated by color of text box) and right-sided grouping in HF network modules, with text indicating module names derived from KEGG and Reactome associations of genes within each module.

We assessed the quality of these measurements in several ways. First, we found that disease status was the dominant source of variation suggesting no major confounding sources of variation

(Supplementary Figure 1). Second, we confirmed enhanced expression of NPPA and NPPB, depletion of SERCA2A, and a shift from MYH7 towards MYH6 expression – established signatures of HF (Figures 3.1A and B). In total, 793 genes were significantly up-regulated in failing hearts compared to non-failing and 848 were down-regulated (fold change greater or lesser than 2 or 0.5 respectively, with $FDR < 0.01$). Finally, as our sample collection was performed immediately before or after cardiac transplantation, (unlike post-mortem samples such as those used in GTex) we investigated whether gene expression programs related to oxidative stress were less perturbed than in samples collected post-mortem. To do this, we compared oxidative stress gene expression as defined by genes in the GO term "Response to oxidative stress" (GO:0006979) in our samples to left ventricular sample data in GTEx, as well as other KEGG and Reactome pathways (data obtained from the recount2 database[44]). Our results suggested that our samples displayed comparable contractility-related gene expression but had significantly less oxidative-stress related gene expression and less perturbation in other metabolic pathways (Figure 3.1C). Having established the quality of our data, we limited our network-based downstream analyses to the 40% genes most variably expressed between failing and non-failing hearts (n=7960) in order to limit inflation of correlation between low covariance gene pairs.

Cardiac co-expression maps reveal dynamic network topology

We inferred undirected, disease-state-specific gene co-expression networks. Gene regulatory network inference from co-expression is a challenging problem that no single method solves adequately in all contexts. Here, we constructed control- and HF- specific networks using methods that rely on gene co-expression (Weighted Gene Co-expression Network Analysis (WGCNA)[84, 85] and Pearson correlation), inverse covariance estimation (Joint Graphical LASSO (JGL) [47]), and mutual information (ARACNe [92] and ZScore). Each of these methods has specific advantages for different questions, e.g. JGL creates a sparser network with the specific intent of reducing representation of non-causal associations, whereas WGCNA relies on denser network topology to capture modules of genes with high likelihood of interaction. Since our downstream analysis required a top-down systems view of coexpression networks, and because we planned to prioritize genes based on the change in connectivity of networks between disease states, we chose to base our subsequent analyses on WGCNA-derived networks, which represent a robust tool for this purpose.[128, 113] To achieve an initial understanding of topological changes between the non-failing and failing heart networks, we compared the structure of modules in each WGCNA-derived network (dendrograms used for module finding shown in Figure 3.4). These networks displayed different structure in HF than in control: First, the number of genes unassigned to any module was much fewer in HF (13 genes were unassigned, compared to 2614 in controls). Second, while each group of genes was specifically enriched with functional annotations as revealed by enrichR [38], the HF modules had more diversity of signaling and metabolic annotations.

We then manually curated modules of genes related to four key processes involved in HF (Figure 3.6B: sarcomeric and contraction genes (orange), excitation-contraction (EC) coupling (red), cardiac remodeling (green), and metabolism (blue)). Network connectivity changed within these process-based modules between non-failing and failing networks. Compared to the non-failing network (grey typeface), the failing heart network (red typeface) saw a general rewiring in connectivity within and between these modules; metabolic genes gained a few specific genes such as the protein phosphatase 1 catalytic and regulatory subunits (PPP1CC, PPP1R1A, and PPP1R3A/B/C) and the muscle 6-phosphofructokinase PFKM in the HF network (Figure 3.6B, blue). Cardiac remodeling genes that gained connectivity were MYBPC3, MYH7, RYR2, and SGCG/D; Sarcomeric and contraction genes that gained connectivity were MYBPC3, MYH7, again listed due to pathway overlaps and VIM, UQCRH/C1; while for EC coupling these were ATP1A1/2/3 and again RYR2.

Finally, plotting a Sankey diagram to observe where module membership changes from controls to HF (Figure 3.6C) revealed large rewiring of co-expression structure. Shared core structure modules such as electron transport chain (ETC) and metabolism genes mostly remained in the same module (dark red in controls and turquoise in HF), while the unassigned genes in the controls (grey) went mostly to the metabolism/ETC (turquoise), cell surface/immune/metabolism (brown), and fibrosis (red) modules in HF.

High quality tissue expression data reveal cardiac eQTLs

We then leveraged genome-wide genotypes to find gene-expression-controlling loci (eQTLs) in each cohort. First, we performed hidden covariate correction using the PEER package (see Methods). We used QTLtools to perform association testing for each cohort separately (see Methods) and performed a scan on the number of hidden factors to correct with PEER [114]. We found that the HF cohort had more associated eQTLs than the control group (1566 vs 936, respectively, with an overlap of 254 loci between the two groups, see http://doi.org/10.5281/zenodo.2617028 for full eQTL results); as expected these eQTLs showed proximity to known transcription factor binding sites and transcription start sites (Figures 3.7A and B). We then tested these eQTLs for enrichment of regulatory associations using RegulomeDB, a database of known and predicted regulatory regions of the genome [33]. Here, both cohorts had several eQTLs with adjacent (within 50 base pair window) regulatory annotation (716/1566 [46%] and 425/936 [45%] of variants, for failing vs control, respectively) and/or predicted for transcription factor binding (Figure 3.2A). We then compared our eQTLs with those found by the GTEx project. Our set of eQTLs contained hundreds of novel associations when compared to the GTEx database for left ventricular tissue: 831/1566 [53% novel associations] for the HF group and 423/936 [45% novel associations] for the control group (Figure 3.7C). We also identified significant overlap with specific tissue types (e.g. artery vs muscle) and cell types (e.g. cultured fibroblasts) (Figure 3.2B).

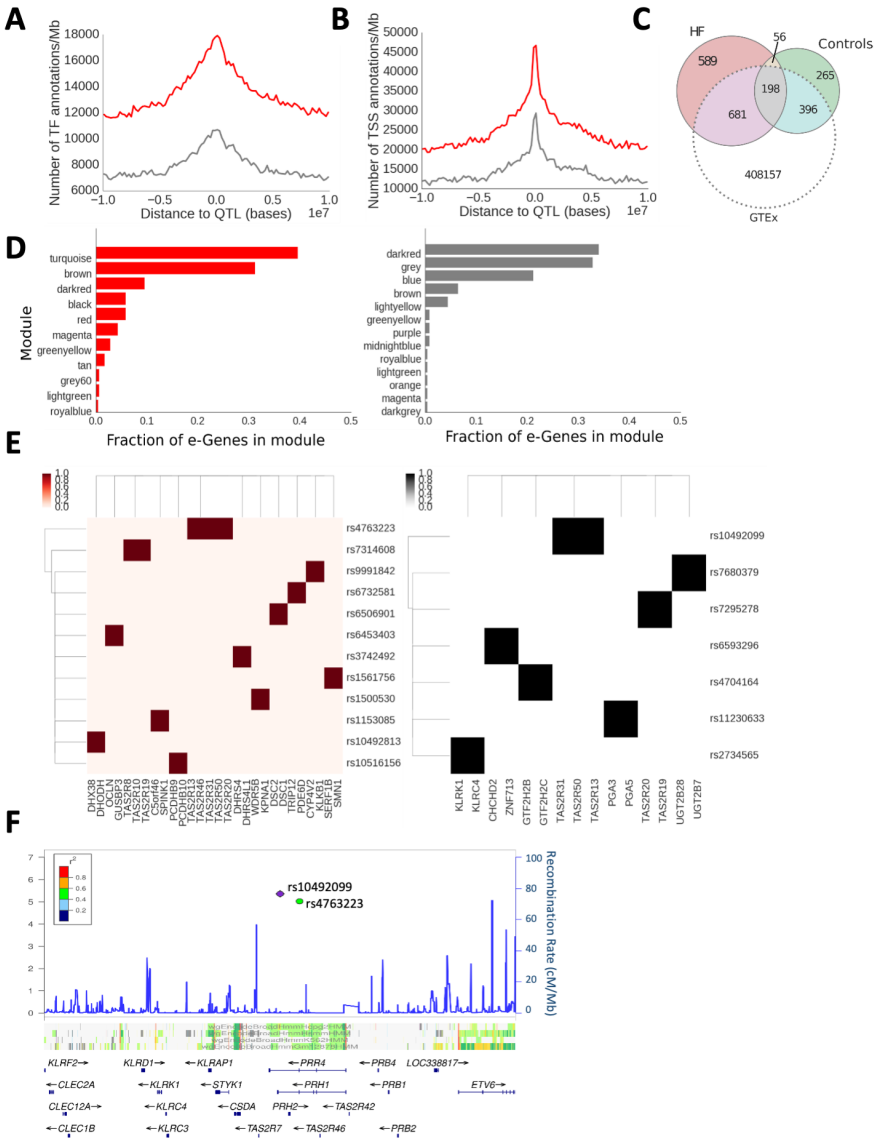


Figure 3.7: Transcription factor (A) and transcription start site (B) annotation to eQTL distance distributions for failing (red) and control hearts. (C) Number of cis eQTLs found for each group that overlapped with GTEx eQTLs. (D) Fraction of modules with genes found to be controlled by at least one eQTL in HF (red, left) and controls (gray, right). (E) Heat map indicators for variants controlling multiple genes in-cis in HF (red, left) and controls (gray, right). In the rows are SNPs controlling genes (columns) colored intensely if the SNP controls the gene. (F) Variants from one locus control a network of G protein coupled receptors TAS2R present in both the failing and control groups.

This percentage of newly identified eQTLs is larger than on previous, related eQTL studies [64, 86], and also displays greater overlap with GTEx than those found in an independent cohort of patients with dilated cardiomyopathy [64]. This large overlap was encouraging, and since we control for known and hidden covariates, our difference in eQTLs compared to related studies may reflect the immediate tissue collection techniques we used, and the difference in disease status (at least one third of cases in this study had ischemic disease, which was not true for comparison studies, which focused on non-ischemic dilated cardiomyopathy [64]).

To assess the physiological impact of our eQTLs, we checked for overlap of our eQTL associations with existing variants in the GWAS catalog [126]. First, we did a simple, direct SNP overlap check with the GWAS variants by (GWAS catalog variants with an LD cutoff of 0.6, using SNiPA [27] to check for LD overlaps). For HF eQTLs, this revealed 41 variants, among which we found 25 associations with sudden cardiac arrest, heart rate variability, and coronary heart disease among other diseases/traits, whereas 33 of the non-failing control eQTLs had associations in the catalog, including QT interval and heart rate variability traits. To assess whether the magnitude of this overlap was higher than expected, we used SNPSNAP [103] to generate two sets of 10000 random variants each with the same LD and gene density characteristics as our failing and non-failing eQTLs. The average overlap of these random sets to GWAS variants was 0.1 for both sets, yielding empirical p-values of less than 0.001 in each set and confirming that our overlap is higher than expected.

To expand our analysis of overlap of our eQTL findings with GWAS, we used eCAVIAR [74], a high-resolution method that leverages SNP density to perform co-localization enrichment tests between hits in a high-powered, publicly available coronary artery disease GWAS and nearby eQTLs from our analysis (see Methods). We chose this coronary artery disease GWAS for comparison not only because it is one of few related to causes of HF that are appropriately powered for this high-resolution method, but believed it to be a reasonable disease surrogate for comparison based on the 36% of explanted failing hearts in our study that had undergone coronary artery bypass grafting (Supplementary Table 1). This method found 7 regions nearby 7 genes that have coronary artery disease associated SNPs and that are significantly co-localized with our eQTLs (see Methods).

We then interrogated which gene modules uncovered by WGCNA were controlled by eQTL loci in concert by examining the fraction of genes that were e-genes of in the eQTL analysis (Figure 3.7C). The modules with the top fraction of e-genes was turquoise in HF and dark red in the controls (40% and 32%, respectively), both of which correspond to electron transport chain and metabolism genes. In HF, the next modules with the most fraction of e-genes were the brown module, a combination of cell surface, immune, and metabolism genes, as well as the dark red module, comprised of muscle contraction and cardiac remodeling genes. For the control cohort, the next module most enriched with e-genes was the grey/unassigned module, indicating a less cohesive regulatory structure; then followed by the blue module dominated by unfolded protein response genes.

We went on to identify modules of coordinating genetic loci and associated networks of genes

within these associations by finding non-trivial connected components (i.e. with more than 3 nodes) within the bipartite association graph of variants and genes, including WGCNA edges with weights larger than the median (Figure 3.7D). Notably, we found two eQTLs within a region enriched with predicted histone modifications that controlled a network of several TAS2R members in cis, a family of G protein-coupled receptors, in both failing and control groups (Figure 3.7E-F, r10492099 and rs4763223). As TAS2R receptors can have high homology in some regions, we checked for potential probe cross-hybridization. We compared sequences for all TAS2R gene probes for the GeneChip ST1.1 array by BLASTing them against human transcript sequences (evalue cutoff of 0.01, with at least 12/25 exact matches). The genes TAS2R43 to TAS2R46 had overlapping, high similarity matching probes, suggesting possible cross-hybridization, while the rest of the receptors' probes were deemed independent by this analysis. These associations, prevalent in both cohorts, highlight a common module of G protein-coupled receptors that have been previously observed to be expressed in the healthy and failing heart [55, 56], and that may play a role in regulation of arrhythmia and contractility [54]. In summary, our heart transplant cardiac samples and inferred gene co-expression networks enabled us to find several previously unidentified cardiac eQTLs in the failing and non-failing heart. Many of the eQTL variants were also associated with cardiac phenotypes in GWAS and some are associated with genes in highly-connected parts of the co-expression network, suggesting coordinated regulation.

Dynamic network topology illuminates central HF regulators

Next, we used our network topology to identify and prioritize genes that were dynamically connected between the failing and control heart networks. Our goal was to identify genes whose network connectivity was increased in the disease state (i.e. HF), but specifically to pathways known to be relevant to the global control of HF mechanisms. We achieved this by ranking genes on two connectivity metrics: i) differential local network connectivity for each gene between control and failing networks, and ii) change in each gene's connectivity globally to HF-relevant molecular pathways manually curated from KEGG and Reactome. We defined local connectivity (LC) as the change in number of edges for each gene between the control and HF networks. Global connectivity (GC) was defined as the number of curated HF-relevant pathways to which each gene was significantly differentially connected in the control vs. HF networks, taking into account network distance (see Methods, Supplementary Figure 5).

Using GC and LC, we assigned each gene to one of four categories (Figure 3.5A): Non-coordinators were genes with decreased LC and GC between the control and HF networks, making them less likely to be highly impactful in the disease state. Local coordinators had significant increases in LC but decreased GC, indicating high co-expression, but mostly with genes unrelated to global HF processes. Pathway coordinators were genes with increased GC but overall low LC, indicating an increased association with global HF processes, but overall low impact with respect to gains in co-expression.

Finally, central coordinators increased both in GC and LC, and therefore represent genes with increased local co-expression involving an increased number of global HF-relevant processes.

After classifying each gene in this way, we focused on central coordinators (Figure 3.5B, top right) in order to capture those genes with the most dynamic connectivity in disease. In addition to increased connectivity with HF-relevant pathways in the HF versus control networks, these central coordinators were enriched in OMIM/KEGG cardiomyopathy terms and pathways (hypertrophic and dilated cardiomyopathy KEGG pathway and OMIM terms, Fisher exact test p-values < 0.001). This includes the myosin binding protein C3 (MYBPC3) which has previously been implicated in the Mendelian cardiac muscle diseases, hypertrophic cardiomyopathy and dilated cardiomyopathy [20, 124] (Figure 3.5B). Particularly, we noted that genes with highest increases in global connectivity regulated HF-related pathways across several cardiomyocyte-relevant processes including metabolism, muscle contraction, and cardiomyopathy-related genes (Figure 3.5C). These data are in concordance with transcriptomic data from murine myocardium with and without exposure to transaortic constriction, which revealed prevalent gene modules associated with mitochondrial and cytoskeletal gene ontologies [86]. In contrast, prioritization by differential gene expression between failing and control myocardium did not reveal many genes genetically associated with known cardiovascular disease pathways. We found no relationship between differential expression and either global or local differential connectivity. Only 1 of the top 20 highly differentially expressed genes was associated with cardiovascular disease pathways in KEGG or Reactome compared to 5 out of the top 20 for the connectivity-derived list – a significant enrichment difference [Fisher exact test p-value < 0.001], Figure 3.1).

Among those central coordinators whose network connectivity was maximally changed in the failing heart was protein phosphatase 1 regulatory subunit 3A (PPP1R3A), with one of the highest changes in GC between control and failing hearts (green typeface, Figure 3.5B)). PPP1R3A, which encodes a muscle-specific regulatory subunit of protein phosphatase 1 (PP1)[76], has not been previously associated with HF. To examine the importance of PPP1R3A to cardiomyocyte hypertrophy across cardiomyopathic etiologies, we also examined its importance in a cardiomyopathy pathway (hypertrophic cardiomyopathy, KEGG), and found that its differential connectivity to this pathway (Figure 3.5D) exceeded even that of MYH7 (Figure 3.5E), an exemplar cardiomyopathy gene. Additionally, we noted that connectivity of PPP1R3A to our lists of sarcomeric and contraction genes was increased significantly in HF (Figure 3.7B). Previous work indicates PPP1R3A contains a glycogen-binding domain [98] and is thought to promote skeletal muscle glycogen synthesis, and variants in PPP1R3A have been associated with decreased insulin sensitivity [51],[116]. Our own networks showed increased connectivity of PPP1R3A to metabolic pathways in control and failing myocardium as well (Figure 3.6B and 3.5C). As cardiac metabolism in HF is known to switch toward a glucose-based metabolism, and as metabolic pathways were significantly connected to PPP1R3A in our HF network (Figure 3.5C), we hypothesized that this gene would play an important role in

the transition from healthy to failing myocardium.

3.1.4 Discussion

We have constructed a comprehensive gene regulatory map of human heart failure (HF). This effort has been facilitated by a systematic approach to the collection of control and failing heart tissue from the operating rooms of cardiac transplant centers and the resulting measurements have allowed us to describe several previously unrecognized molecular features of HF. Notably, the network structure of HF differs markedly from that of non-failing heart tissue. Specifically, we find that the control network has a large number of genes (2614) not associated with modules, whereas in the HF network, only 13 genes remained unassociated, providing evidence for increased connectivity in the HF network. Further, in the HF network, there is significant rewiring of genes to new processes (Figure 3.6C), and an array of changes in co-expression relationships of central genes to key processes such as sarcomeric structure, excitation-contraction coupling, metabolism, and cardiac remodeling.

The inferred networks also aided in the discovery of new eQTLs in the non-failing and failing contexts. Notably, we found a greater number of eQTLs in the failing heart, half of which were not previously reported, but that were still implicated in higher phenotype associations in GWAS. In some cases, the expression of local subnetworks of genes were found to be associated with one locus, such as several members of the TAS2R G protein coupled receptor family, receptors typically associated with the sensation of taste but recently found to be variously expressed in cardiac tissue.[55] Further, these eQTLs were enriched for regulatory annotations, which were more prevalent in the failing heart cohort. Thus, these newly identified eQTLs are not only important for identifying potential regulatory DNA, but also novel molecular actors in HF that would not have been discovered in healthy tissue alone.

In addition to identified eQTLs, comparison of co-expression structure between disease and control networks highlighted genes whose connectivity changed meaningfully between the two cohorts, regardless of change in mean expression. This reveals central coordinating genes in HF that would otherwise be missed by examination of individual gene expression alone. This phenomenon has been observed across human diseases,[75, 129] and highlights a critical feature of co-expression networks: they capture the global complexity of regulation beyond individual changes in expression to identify genes pivotal in disease. Here, our strategy classified genes both by their local connectivity and their network distance to HF-relevant pathways (global connectivity) to identify PPP1R3A as a gene with a putative role in HF. PPP1R3A would not have been identified without this network approach, given that its own expression is not altered drastically in disease. Subsequent molecular investigations demonstrated its effect on other central coordinators between the control and HF networks as well as a deleterious effect on contractile function in the setting of pressure overload in vivo. Although this gene has not previously been associated with human cardiac disease, studies in both mouse and human have found that loss-of-function mutations in PPP1R3A manipulate metabolic

pathways in skeletal muscle, and our own analysis implicated it in pyruvate, and other metabolic pathways (Figure 3.5C) [116, 109]. Elimination of PPP1R3A in a murine model of cardiomyopathy revealed a maladaptive role for this gene in HF, and our in vitro studies highlight the metabolic switch of failing myocardium: toward inefficient glycolytic glucose metabolism and away from the use of pyruvate in respiratory metabolism (Figure 3.8D).

While a great strength of this study is its immediate isolation of RNA from freshly explanted human tissue, the resultant networks are not based on gene expression from a single cell type, but rather whole cardiac tissue. While the expression-based networks we use lend themselves to the construction of networks that bridge cell types, we cannot state with certainty that the identified central coordinators are resultant of gene-gene interactions within cardiomyocytes alone, though many of them changed significantly with PPP1R3A knockdown in NRVMs (Figure 3.8A). In the same vein, as the causes of HF leading to transplant are diverse, the network-based hypotheses generated by this work are likely to highlight final common pathways of HF resulting from diverse etiologies. This can be viewed as a strength of this work as it is applicable across these multiple etiologies, however, additional studies investigating the early stages of specific HF etiologies will add equally to the literature in future. It must also be noted that, due to the nature of the cohort of control hearts available for transplant, control hearts here are not free of disease (e.g. diabetes, Supplementary Table 1). Though there are more male hearts included in the HF group than control hearts, principal component analysis of gene expression does not reveal segregation by sex (Supplementary Figure 3.6). Nevertheless, we controlled for this variable in both the network and eQTL analyses.

Since genome-wide expression studies were introduced, there has been interest in quantifying genes that are significantly differentially expressed, e.g. between failing and non-failing states. What this linear, unitary approach fails to capture are mechanisms influencing higher order phenotypes reflected in re-wiring of transcriptional partners that do not affect expression levels of specific genes. Earlier work has already led to the discovery of central genes using co-expression changes [49, 127]. Here, we expanded this use of gene co-expression by exploiting not only gene interaction degree, but also integrated topological network differences and known pathway information. In our HF networks, we have shown how differences between these network topology properties in failing and non-failing hearts can be used to uncover novel mechanisms and highlight new putative therapeutic targets.

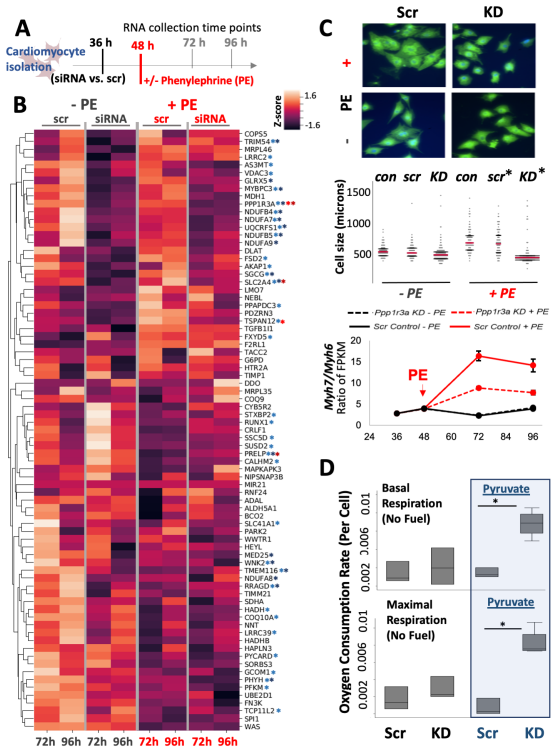


Figure 3.8: (A) Experimental design: NRVMs were isolated, transfected with siRNA 36 hours later. Phenylephrine or vehicle treatment started at 48 hours. RNA was collected at 36, 48, 72 and 96 hours after isolation. (B) Clustered heat map of NRVM transcriptional expression of central coordinators in response to PPP1R3A knockdown (measured by RNAseq). Expression is shown from NRVMs at 72 and 96 hours after isolation normalized to pre-treatment expression, and displayed as per-gene z-scores. Data from cells with and without phenylephrine (PE) are shown on the left and right sides of the heat map with and without siRNA knockdown as indicated. Stars indicate central coordinators significantly differentially regulated by PPP1R3a knockdown (FDR¡0.05, red stars indicate significance in the PE treated group (red at 72 hours, dark red at 96 hours) and blue stars indicate significance in the untreated group after PPP1R3a knockdown at 72 (light blue) and 96 (dark blue) hours). (C) PPP1R3A knockdown protects against hypertrophic stimulus of phenylephrine treatment. Upper Panel: Cell size measurements of a sample of cells under phenylephrine and normal conditions, with and without PPP1R3a KD reveal reduced hypertrophy in NRVMs treated with PE and PPP1R3a KD compared to PE treated cells with and without scramble siRNA transfection ($p < 1e10^{-4}$ (ANOVA), *=$p < 1e10^{-3}$ by Bonferroni posttest. n=100 cells for each group, Red bars indicate mean, black bars indicate one standard deviation). Lower panel: MYH7/MYH6 ratio, a marker for HF, is decreased in PPP1R3a knockdown NRVMs treated with PE compared to those transfected with scrambled siRNA control at 72 hours and 96 hours after isolation ($p < 1e10^{-}2$ for both comparisons, error bars represent 95% confidence intervals). (D) Respiratory pyruvate metabolism increases after PPP1R3A knockdown. Knockdown of PPP1R3A leads to increased basal and maximal respiratory metabolism of pyruvate as measured by oxygen consumption in NRVM (basal respiration: p=0.02, maximal respiration: p=0.005, center line indicates median, box indicates IQR, and whiskers indicate next adjacent value. n= 3 biologically independent samples for the siRNA/pyruvate group and n=4 for all other groups).

Bibliography

[1] 2010 census summary file 1— technical documentation.

[2] Considerations for phased implementation of COVID-19 vaccination, 2021. publisher: Centers for Disease Control and Prevention.

[3] COVID data tracker. publisher: Centers for Disease Control and Prevention.

[4] Improving california's prison inmate classification system.

[5] Monthly Total Population Report Archive. publisher: California Department of Corrections and Rehabilitation.

[6] People with Certain Medical Conditions. publisher: Centers for Disease Control and Prevention.

[7] Topline report on COVID-19 vaccination in the United States. Technical report, The Delphi Group at Carnegie Mellon University in partnership with Facebook.

[8] Academic and Vocational Education Programs Progress Report. Technical report, California Department of Corrections and Rehabilitation, February 2009.

[9] 15. Interim Guidance on Management of Coronavirus Disease 2019 (COVID-19) in Correctional and Detention Facilities, October 2020. publisher: Centers for Disease Control and Prevention.

[10] CDC COVID Data Tracker, November 2020.

[11] Continuing Education, November 2020. publisher: California Department of Corrections and Rehabilitation.

[12] COVID-19 Guidance for Shared or Congregate Housing, August 2020. publisher: Centers for Disease Control and Prevention.

[13] Death row USA – quarterly reports. Technical report, Legal Defense and Educational Fund, National Association for the Advancement of Colored People, 2020.

[14] A state-by-state look at 15 months of coronavirus in prisons, May 2020.

[15] Bnt162b2 mrna covid-19 vaccine in a nationwide mass vaccination setting. *New England Journal of Medicine*, 384(20):1968–1970, May 2021.

[16] Cases and Deaths, August 2021. publisher: California COVID-19 Dashboard.

[17] Population COVID-19 Tracking: COVID-19 Trends, August 2021. publisher: California Department of Corrections and Rehabilitation.

[18] Safety and efficacy of the bnt162b2 mrna covid-19 vaccine. *New England Journal of Medicine*, 384(16):1576–1578, April 2021.

[19] Tracking Variants: How has the proportion of variants of concern and variants of interest in California changed over time?, August 2021. publisher: California Department of Public Health.

[20] L. E. Alday and E. Moreyra. Secondary hypertrophic cardiomyopathy in infancy and childhood. *American Heart Journal*, 108(4 Pt 1):996–1000, October 1984.

[21] Kashif Ali, Gary Berman, Honghong Zhou, Weiping Deng, Veronica Faughnan, Maria Coronado-Voges, Baoyu Ding, Jacqueline Dooley, Bethany Girard, William Hillebrand, Rolando Pajon, Jacqueline M. Miller, Brett Leav, and Roderick McPhee. Evaluation of mrna-1273 sars-cov-2 vaccine in adolescents. *The New England Journal of Medicine*, 385(24):2241–2251, December 2021.

[22] Kiran Ali, Sanjana Rao, Gilbert Berdine, Victor Test, and Kenneth Nugent. Retracted: a retrospective analysis and comparison of prisoners and community-based patients with covid-19 requiring intensive care during the first phase of the pandemic in west texas. *Journal of Primary Care & Community Health*, 11:215013272095468, January 2020.

[23] Marcella Alsan and Marianne Wanamaker. Tuskegee and the health of black men. *The quarterly journal of economics*, 133(1):407–455, February 2018.

[24] P. K. Andersen and R. D. Gill. Cox's regression model for counting processes: a large sample study. *The Annals of Statistics*, 10(4), December 1982.

[25] Yoel Angel, Avishay Spitzer, Oryan Henig, Esther Saiag, Eli Sprecher, Hagit Padova, and Ronen Ben-Ami. Association between vaccination with bnt162b2 and incidence of symptomatic and asymptomatic sars-cov-2 infections among health care workers. *JAMA*, 325(24):2457–2465, June 2021.

[26] Sweta Haldar Published: Apr 07 and 2022. Latest data on covid-19 vaccinations by race/ethnicity, April 2022.

[27] Matthias Arnold, Johannes Raffler, Arne Pfeufer, Karsten Suhre, and Gabi Kastenmüller. SNiPA: an interactive, genetic variant-centered annotation browser. *Bioinformatics*, 31(8):1334–1336, April 2015.

[28] Sachini Bandara, Alene Kennedy-Hendricks, Sydney Merritt, Colleen L. Barry, and Brendan Saloner. Early effects of covid-19 on programs providing medications for opioid use disorder in jails and prisons. *Journal of Addiction Medicine*, 14(5):e257–e260, September 2020.

[29] Benjamin A. Barsky, Eric Reinhart, Paul Farmer, and Salmaan Keshavjee. Vaccination plus decarceration — stopping covid-19 in jails and prisons. *New England Journal of Medicine*, 384(17):1583–1585, April 2021.

[30] Ramona Benkert, Adolfo Cuevas, Hayley S. Thompson, Emily Dove-Meadows, and Donulae Knuckles. Ubiquitous yet unclear: a systematic review of medical mistrust. *Behavioral Medicine (Washington, D.C.)*, 45(2):86–101, June 2019.

[31] Christian Benner, Chris C.A. Spencer, Aki S. Havulinna, Veikko Salomaa, Samuli Ripatti, and Matti Pirinen. FINEMAP: efficient variable selection using summary data from genome-wide association studies. *Bioinformatics*, 32(10):1493–1501, May 2016.

[32] Laura M. Bogart, Yusuf Ransome, Wanda Allen, Molly Higgins-Biddle, and Bisola O. Ojikutu. Hiv-related medical mistrust, hiv testing, and hiv risk in the national survey on hiv in the black community. *Behavioral Medicine (Washington, D.C.)*, 45(2):134–142, June 2019.

[33] Alan P. Boyle, Eurie L. Hong, Manoj Hariharan, Yong Cheng, Marc A. Schaub, Maya Kasowski, Konrad J. Karczewski, Julie Park, Benjamin C. Hitz, Shuai Weng, J. Michael Cherry, and Michael Snyder. Annotation of functional variation in personal genomes using RegulomeDB. *Genome Research*, 22(9):1790–1797, September 2012.

[34] Amadea Britton, Kara M. Jacobs Slifka, Chris Edens, Srinivas Acharya Nanduri, Stephen M. Bart, Nong Shang, Adora Harizaj, Jillian Armstrong, Kerui Xu, Hanna Y. Ehrlich, Elizabeth Soda, Gordana Derado, Jennifer R. Verani, Stephanie J. Schrag, John A. Jernigan, Vivian H. Leung, and Sunil Parikh. Effectiveness of the pfizer-biontech covid-19 vaccine among residents of two skilled nursing facilities experiencing covid-19 outbreaks - connecticut, december 2020-february 2021. *MMWR. Morbidity and mortality weekly report*, 70(11):396–401, March 2021.

[35] Thomas P. Cappola and Kenneth B. Margulies. Functional genomics applied to cardiovascular medicine. *Circulation*, 124(1):87–94, July 2011.

[36] Elizabeth D. Carlson and Robert M. Chamberlain. The Black-White perception gap and health disparities research. *Public Health Nursing (Boston, Mass.)*, 21(4):372–379, August 2004.

[37] Alyson M. Cavanaugh, Sarah Fortier, Patricia Lewis, Vaneet Arora, Matt Johnson, Karim George, Joshua Tobias, Stephanie Lunn, Taylor Miller, Douglas Thoroughman, and Kevin B. Spicer. Covid-19 outbreak associated with a sars-cov-2 r. 1 lineage variant in a skilled nursing facility after vaccination program — kentucky, march 2021. *MMWR. Morbidity and Mortality Weekly Report*, 70(17):639–643, April 2021.

[38] Edward Y Chen, Christopher M Tan, Yan Kou, Qiaonan Duan, Zichen Wang, Gabriela Vaz Meirelles, Neil R Clark, and Avi Ma'ayan. Enrichr: interactive and collaborative HTML5 gene list enrichment analysis tool. *BMC Bioinformatics*, 14(1):128, December 2013.

[39] Mary M. Chen, Euan A. Ashley, David X. F. Deng, Anya Tsalenko, Alicia Deng, Raymond Tabibiazar, Amir Ben-Dor, Brett Fenster, Eugene Yang, Jennifer Y. King, Michael Fowler, Robert Robbins, Frances L. Johnson, Laurakay Bruhn, Theresa McDonagh, Henry Dargie, Zohar Yakhini, Philip S. Tsao, and Thomas Quertermous. Novel role for the potent endogenous inotrope apelin in human cardiac dysfunction. *Circulation*, 108(12):1432–1439, September 2003.

[40] Elizabeth T. Chin, David Leidner, Theresa Ryckman, Yiran E. Liu, Lea Prince, Fernando Alarid-Escudero, Jason R. Andrews, Joshua A. Salomon, Jeremy D. Goldhaber-Fiebert, and David M. Studdert. Covid-19 vaccine acceptance in california state prisons. *The New England Journal of Medicine*, 385(4):374–376, July 2021.

[41] Elizabeth T. Chin, Theresa Ryckman, Lea Prince, David Leidner, Fernando Alarid-Escudero, Jason R. Andrews, Joshua A. Salomon, David M. Studdert, and Jeremy D. Goldhaber-Fiebert. Covid-19 in the california state prison system: an observational study of decarceration, ongoing risks, and risk factors. *Journal of General Internal Medicine*, 36(10):3096–3102, October 2021.

[42] Elizabeth T. Chin, Theresa Ryckman, Lea Prince, David Leidner, Fernando Alarid-Escudero, Jason R. Andrews, Joshua A. Salomon, David M. Studdert, and Jeremy D. Goldhaber-Fiebert. Covid-19 in the california state prison system: an observational study of decarceration, ongoing risks, and risk factors. *Journal of General Internal Medicine*, 36(10):3096–3102, October 2021.

[43] David H. Cloud, Cyrus Ahalt, Dallas Augustine, David Sears, and Brie Williams. Medical isolation and solitary confinement: balancing health and humanity in us jails and prisons during covid-19. *Journal of General Internal Medicine*, 35(9):2738–2742, September 2020.

[44] Leonardo Collado-Torres, Abhinav Nellore, Kai Kammers, Shannon E Ellis, Margaret A Taub, Kasper D Hansen, Andrew E Jaffe, Ben Langmead, and Jeffrey T Leek. Reproducible RNA-seq analysis using recount2. *Nature Biotechnology*, 35(4):319–321, April 2017.

[45] Committee on the Best Practices for Implementing Decarceration as a Strategy to Mitigate the Spread of COVID-19 in Correctional Facilities, Committee on Law and Justice, Division

of Behavioral and Social Sciences and Education, and National Academies of Sciences, Engineering, and Medicine. *Decarcerating correctional facilities during covid-19: advancing health, equity, and safety*. National Academies Press, Washington, D.C., December 2020.

[46] Committee on the Best Practices for Implementing Decarceration as a Strategy to Mitigate the Spread of COVID-19 in Correctional Facilities, Committee on Law and Justice, Division of Behavioral and Social Sciences and Education, and National Academies of Sciences, Engineering, and Medicine. *Decarcerating correctional facilities during covid-19: advancing health, equity, and safety*. National Academies Press, Washington, D.C., December 2020.

[47] Patrick Danaher, Pei Wang, and Daniela M. Witten. The joint graphical lasso for inverse covariance estimation across multiple classes. *Journal of the Royal Statistical Society: Series B (Statistical Methodology)*, 76(2):373–397, March 2014.

[48] Olivier Delaneau, Halit Ongen, Andrew A. Brown, Alexandre Fort, Nikolaos I. Panousis, and Emmanouil T. Dermitzakis. A complete tool set for molecular QTL discovery and analysis. *Nature Communications*, 8:15452, May 2017.

[49] Frederick E. Dewey, Marco V. Perez, Matthew T. Wheeler, Clifton Watt, Joshua Spin, Peter Langfelder, Steve Horvath, Sridhar Hannenhalli, Thomas P. Cappola, and Euan A. Ashley. Gene coexpression network topology of cardiac development, hypertrophy, and failure. *Circulation. Cardiovascular Genetics*, 4(1):26–35, February 2011.

[50] Alexander Dobin, Carrie A. Davis, Felix Schlesinger, Jorg Drenkow, Chris Zaleski, Sonali Jha, Philippe Batut, Mark Chaisson, and Thomas R. Gingeras. STAR: ultrafast universal RNA-seq aligner. *Bioinformatics (Oxford, England)*, 29(1):15–21, January 2013.

[51] M. P. Egloff, D. F. Johnson, G. Moorhead, P. T. Cohen, P. Cohen, and D. Barford. Structural basis for the recognition of regulatory subunits by the catalytic subunit of protein phosphatase 1. *The EMBO journal*, 16(8):1876–1887, April 1997.

[52] Howard Eisen, editor. *Heart failure: a comprehensive guide to pathophysiology and clinical care*. Springer London, London, 2017.

[53] M. Watt Espy and John Ortiz Smykla. Executions in the united states, 1608-2002: the espy file: version 5, 1988. Type: dataset.

[54] Simon R. Foster, Kristina Blank, Louise E. See Hoe, Maik Behrens, Wolfgang Meyerhof, Jason N. Peart, and Walter G. Thomas. Bitter taste receptor agonists elicit G-protein-dependent negative inotropy in the murine heart. *The FASEB Journal*, 28(10):4497–4508, October 2014.

[55] Simon R. Foster, Enzo R. Porrello, Brooke Purdue, Hsiu-Wen Chan, Anja Voigt, Sabine Frenzel, Ross D. Hannan, Karen M. Moritz, David G. Simmons, Peter Molenaar, Eugeni

Roura, Ulrich Boehm, Wolfgang Meyerhof, and Walter G. Thomas. Expression, regulation and putative nutrient-sensing function of taste gpcrs in the heart. *PLoS ONE*, 8(5):e64579, May 2013.

[56] Simon R. Foster, Enzo R. Porrello, Maurizio Stefani, Nicola J. Smith, Peter Molenaar, Cristobal G. dos Remedios, Walter G. Thomas, and Mirana Ramialison. Cardiac gene expression data and in silico analysis provide novel insights into human and mouse taste receptor gene regulation. *Naunyn-Schmiedeberg's Archives of Pharmacology*, 388(10):1009–1027, October 2015.

[57] Cary Funk and Alec Tyson. Intent to get a covid-19 vaccine rises to 60% as confidence in research and development process increases, December 2020.

[58] Radhika Gharpure, Angela Guo, Courtney Krier Bishnoi, Urvi Patel, David Gifford, Ashley Tippins, Aaron Jaffe, Evan Shulman, Nimalie Stone, Elisabeth Mungai, Suparna Bagchi, Jeneita Bell, Arjun Srinivasan, Anita Patel, and Ruth Link-Gelles. Early covid-19 first-dose vaccination coverage among residents and staff members of skilled nursing facilities participating in the pharmacy partnership for long-term care program - united states, december 2020-january 2021. *MMWR. Morbidity and mortality weekly report*, 70(5):178–182, February 2021.

[59] Radhika Gharpure, Anita Patel, and Ruth Link-Gelles. First-dose covid-19 vaccination coverage among skilled nursing facility residents and staff. *JAMA*, 325(16):1670, April 2021.

[60] M. Gabriela M. Gomes, Stephen B. Gordon, and David G. Lalloo. Clinical trials: The mathematics of falling vaccine efficacy with rising disease incidence. *Vaccine*, 34(27):3007–3009, June 2016.

[61] GTEx Consortium. Human genomics. The Genotype-Tissue Expression (Gtex) pilot analysis: multitissue gene regulation in humans. *Science (New York, N.Y.)*, 348(6235):648–660, May 2015.

[62] GTEx Consortium, Laboratory, Data Analysis &Coordinating Center (LDACC)—Analysis Working Group, Statistical Methods groups—Analysis Working Group, Enhancing GTEx (eGTEx) groups, NIH Common Fund, NIH/NCI, NIH/NHGRI, NIH/NIMH, NIH/NIDA, Biospecimen Collection Source Site—NDRI, Biospecimen Collection Source Site—RPCI, Biospecimen Core Resource—VARI, Brain Bank Repository—University of Miami Brain Endowment Bank, Leidos Biomedical—Project Management, ELSI Study, Genome Browser Data Integration &Visualization—EBI, Genome Browser Data Integration &Visualization—UCSC Genomics Institute, University of California Santa Cruz, Lead analysts:, Laboratory, Data Analysis &Coordinating Center (LDACC):, NIH program management:, Biospecimen collection:, Pathology:, eQTL manuscript working group:, Alexis Battle, Christopher D. Brown, Barbara E.

Engelhardt, and Stephen B. Montgomery. Genetic effects on gene expression across human tissues. *Nature*, 550(7675):204–213, October 2017.

[63] Eric J. Haas, Frederick J. Angulo, John M. McLaughlin, Emilia Anis, Shepherd R. Singer, Farid Khan, Nati Brooks, Meir Smaja, Gabriel Mircus, Kaijie Pan, Jo Southern, David L. Swerdlow, Luis Jodar, Yeheskel Levy, and Sharon Alroy-Preis. Impact and effectiveness of mRNA BNT162b2 vaccine against SARS-CoV-2 infections and COVID-19 cases, hospitalisations, and deaths following a nationwide vaccination campaign in Israel: an observational study using national surveillance data. *The Lancet*, 397(10287):1819–1829, May 2021.

[64] Jan Haas, Stefan Mester, Alan Lai, Karen S. Frese, Farbod Sedaghat-Hamedani, Elham Kayvanpour, Tobias Rausch, Rouven Nietsch, Jes-Niels Boeckel, Avisha Carstensen, Mirko Völkers, Carsten Dietrich, Dietmar Pils, Ali Amr, Daniel B. Holzer, Diana Martins Bordalo, Daniel Oehler, Tanja Weis, Derliz Mereles, Sebastian Buss, Eva Riechert, Emil Wirsz, Maximilian Wuerstle, Jan O. Korbel, Andreas Keller, Hugo A. Katus, Andreas E. Posch, and Benjamin Meder. Genomic structural variations lead to dysregulation of important coding and non-coding RNA species in dilated cardiomyopathy. *EMBO molecular medicine*, 10(1):107–120, January 2018.

[65] Liesl M. Hagan, Samantha P. Williams, Anne C. Spaulding, Robin L. Toblin, Jessica Figlenski, Jeanne Ocampo, Tara Ross, Heidi Bauer, Justine Hutchinson, Kimberley D. Lucas, Matthew Zahn, Chun Chiang, Timothy Collins, Alexis Burakoff, Juli Bettridge, Ginger Stringer, Randolph Maul, Kristen Waters, Courtney Dewart, Jennifer Clayton, Sietske de Fijter, Radha Sadacharan, Linda Garcia, Naomi Lockett, Kirstin Short, Laxman Sunder, and Senad Handanagic. Mass testing for sars-cov-2 in 16 prisons and jails - six jurisdictions, united states, april-may 2020. *MMWR. Morbidity and mortality weekly report*, 69(33):1139–1143, August 2020.

[66] Pei Han, Wei Li, Chiou-Hong Lin, Jin Yang, Ching Shang, Sylvia T. Nuernberg, Kevin Kai Jin, Weihong Xu, Chieh-Yu Lin, Chien-Jung Lin, Yiqin Xiong, Huanchieh Chien, Bin Zhou, Euan Ashley, Daniel Bernstein, Peng-Sheng Chen, Huei-Sheng Vincent Chen, Thomas Quertermous, and Ching-Pin Chang. A long noncoding RNA protects the heart from pathological hypertrophy. *Nature*, 514(7520):102–106, October 2014.

[67] Sridhar Hannenhalli, Mary E. Putt, Joan M. Gilmore, Junwen Wang, Michael S. Parmacek, Jonathan A. Epstein, Edward E. Morrisey, Kenneth B. Margulies, and Thomas P. Cappola. Transcriptional genomics associates FOX transcription factors with human heart failure. *Circulation*, 114(12):1269–1276, September 2006.

[68] Paul A. Harris, Robert Taylor, Robert Thielke, Jonathon Payne, Nathaniel Gonzalez, and Jose G. Conde. Research electronic data capture (Redcap)—A metadata-driven methodology

and workflow process for providing translational research informatics support. *Journal of Biomedical Informatics*, 42(2):377–381, April 2009.

[69] Laura Hawks, Steffie Woolhandler, and Danny McCormick. Covid-19 in prisons and jails in the united states. *JAMA Internal Medicine*, 180(8):1041, August 2020.

[70] Matthias Heinig, Michiel E. Adriaens, Sebastian Schafer, Hanneke W. M. van Deutekom, Elisabeth M. Lodder, James S. Ware, Valentin Schneider, Leanne E. Felkin, Esther E. Creemers, Benjamin Meder, Hugo A. Katus, Frank Rühle, Monika Stoll, François Cambien, Eric Villard, Philippe Charron, Andras Varro, Nanette H. Bishopric, Alfred L. George, Cristobal Dos Remedios, Aida Moreno-Moral, Francesco Pesce, Anja Bauerfeind, Franz Rüschendorf, Carola Rintisch, Enrico Petretto, Paul J. Barton, Stuart A. Cook, Yigal M. Pinto, Connie R. Bezzina, and Norbert Hubner. Natural genetic variation of the cardiac transcriptome in non-diseased donors and patients with dilated cardiomyopathy. *Genome Biology*, 18(1):170, September 2017.

[71] Brandy F. Henry. Social distancing and incarceration: policy and management strategies to reduce covid-19 transmission and promote health equity through decarceration. *Health Education & Behavior*, 47(4):536–539, August 2020.

[72] Matt D. T. Hitchings, Joseph A. Lewnard, Natalie E. Dean, Albert I. Ko, Otavio T. Ranzani, Jason R. Andrews, and Derek A. T. Cummings. Use of recently vaccinated individuals to detect bias in test-negative case-control studies of COVID-19 vaccine effectiveness. *Epidemiology (Cambridge, Mass.)*, April 2022.

[73] Kelly M. Hoffman, Sophie Trawalter, Jordan R. Axt, and M. Norman Oliver. Racial bias in pain assessment and treatment recommendations, and false beliefs about biological differences between blacks and whites. *Proceedings of the National Academy of Sciences*, 113(16):4296–4301, April 2016.

[74] Farhad Hormozdiari, Martijn van de Bunt, Ayellet V. Segrè, Xiao Li, Jong Wha J. Joo, Michael Bilow, Jae Hoon Sul, Sriram Sankararaman, Bogdan Pasaniuc, and Eleazar Eskin. Colocalization of gwas and eqtl signals detects target genes. *American Journal of Human Genetics*, 99(6):1245–1260, December 2016.

[75] Tianxiao Huan, Bin Zhang, Zhi Wang, Roby Joehanes, Jun Zhu, Andrew D. Johnson, Saixia Ying, Peter J. Munson, Nalini Raghavachari, Richard Wang, Poching Liu, Paul Courchesne, Shih-Jen Hwang, Themistocles L. Assimes, Ruth McPherson, Nilesh J. Samani, Heribert Schunkert, Coronary ARteryDIsease Genome wide Replication and Meta-analysis (CARDIoGRAM) Consortium, International Consortium for Blood Pressure GWAS (ICBP), Qingying Meng, Christine Suver, Christopher J. O'Donnell, Jonathan Derry, Xia Yang, and Daniel Levy. A systems biology framework identifies molecular underpinnings of coronary heart disease. *Arteriosclerosis, Thrombosis, and Vascular Biology*, 33(6):1427–1434, June 2013.

[76] M. J. Hubbard and P. Cohen. Regulation of protein phosphatase-1G from rabbit skeletal muscle. 2. Catalytic subunit translocation is a mechanism for reversible inhibition of activity toward glycogen-bound substrates. *European Journal of Biochemistry*, 186(3):711–716, December 1989.

[77] Prison Policy Initiative. Incarcerated people and corrections staff should be prioritized in COVID-19 vaccination plans.

[78] Monik C. Jiménez, Tori L. Cowger, Lisa E. Simon, Maya Behn, Nicole Cassarino, and Mary T. Bassett. Epidemiology of covid-19 among incarcerated individuals and staff in massachusetts jails and prisons. *JAMA Network Open*, 3(8):e2018851, August 2020.

[79] Dhruv S. Kazi and Daniel B. Mark. The economics of heart failure. *Heart Failure Clinics*, 9(1):93–106, January 2013.

[80] Byron S. Kennedy, Robert P. Richeson, and Amy J. Houde. Risk factors for sars-cov-2 in a statewide correctional system. *New England Journal of Medicine*, 383(25):2479–2480, December 2020.

[81] Michelle M. Kittleson, Khalid M. Minhas, Rafael A. Irizarry, Shui Q. Ye, Gina Edness, Elayne Breton, John V. Conte, Gordon Tomaselli, Joe G. N. Garcia, and Joshua M. Hare. Gene expression analysis of ischemic and nonischemic cardiomyopathy: shared and distinct genes in the development of heart failure. *Physiological Genomics*, 21(3):299–307, May 2005.

[82] Ann Hinga Klein and Derek M. Norman. Covid outbreaks devastated prisons, but state inmates' access to the vaccine varies widely. *The New York Times*, March 2021.

[83] Uzay Kırbıyık, Alison M. Binder, Isaac Ghinai, Chad Zawitz, Rebecca Levin, Usha Samala, Michelle Bryant Smith, Jane Gubser, Bridgette Jones, Kate Varela, Josh Rafinski, Anne Fitzgerald, Peter Orris, Alex Bahls, Sharon Welbel, Connie Mennella, Stephanie R. Black, and Paige A. Armstrong. Network characteristics and visualization of covid-19 outbreak in a large detention facility in the united states — cook county, illinois, 2020. *MMWR. Morbidity and Mortality Weekly Report*, 69(44):1625–1630, November 2020.

[84] Peter Langfelder and Steve Horvath. WGCNA: an R package for weighted correlation network analysis. *BMC Bioinformatics*, 9(1):559, December 2008.

[85] Peter Langfelder and Steve Horvath. Fast R functions for robust correlations and hierarchical clustering. *Journal of Statistical Software*, 46(11), 2012.

[86] Jae-Hyung Lee, Chen Gao, Guangdun Peng, Christopher Greer, Shuxun Ren, Yibin Wang, and Xinshu Xiao. Analysis of transcriptome complexity through rna sequencing in normal and failing murine hearts. *Circulation Research*, 109(12):1332–1341, December 2011.

[87] Joseph A. Lewnard, Christine Tedijanto, Benjamin J. Cowling, and Marc Lipsitch. Measurement of vaccine direct effects under the test-negative design. *American Journal of Epidemiology*, 187(12):2686–2697, December 2018.

[88] Xin Li, Yungil Kim, Emily K. Tsang, Joe R. Davis, Farhan N. Damani, Colby Chiang, Gaelen T. Hess, Zachary Zappala, Benjamin J. Strober, Alexandra J. Scott, Amy Li, Andrea Ganna, Michael C. Bassik, Jason D. Merker, GTEx Consortium, Laboratory, Data Analysis &Coordinating Center (LDACC)—Analysis Working Group, Statistical Methods groups—Analysis Working Group, Enhancing GTEx (eGTEx) groups, NIH Common Fund, NIH/NCI, NIH/NHGRI, NIH/NIMH, NIH/NIDA, Biospecimen Collection Source Site—NDRI, Biospecimen Collection Source Site—RPCI, Biospecimen Core Resource—VARI, Brain Bank Repository—University of Miami Brain Endowment Bank, Leidos Biomedical—Project Management, ELSI Study, Genome Browser Data Integration &Visualization—EBI, Genome Browser Data Integration &Visualization—UCSC Genomics Institute, University of California Santa Cruz, Ira M. Hall, Alexis Battle, and Stephen B. Montgomery. The impact of rare variation on gene expression across tissues. *Nature*, 550(7675):239–243, October 2017.

[89] Lunna Lopes and 2021. Vaccine hesitancy among hispanic adults, January 2021.

[90] Tarub S. Mabud, Maria de Lourdes Delgado Alves, Albert I. Ko, Sanjay Basu, Katharine S. Walter, Ted Cohen, Barun Mathema, Caroline Colijn, Everton Lemos, Julio Croda, and Jason R. Andrews. Evaluating strategies for control of tuberculosis in prisons and prevention of spillover into communities: An observational and modeling study from Brazil. *PLOS Medicine*, 16(1):e1002737, January 2019.

[91] Morgan Maner. An analysis of interim covid-19 vaccination plans, August 2021.

[92] Adam A Margolin, Ilya Nemenman, Katia Basso, Chris Wiggins, Gustavo Stolovitzky, Riccardo Dalla Favera, and Andrea Califano. Aracne: an algorithm for the reconstruction of gene regulatory networks in a mammalian cellular context. *BMC Bioinformatics*, 7(S1):S7, March 2006.

[93] Kenneth B. Margulies, Daniel P. Bednarik, and Daniel L. Dries. Genomics, transcriptional profiling and heart failure. *Journal of the American College of Cardiology*, 53(19):1752–1759, May 2009.

[94] Benjamin Meder, Jan Haas, Farbod Sedaghat-Hamedani, Elham Kayvanpour, Karen Frese, Alan Lai, Rouven Nietsch, Christina Scheiner, Stefan Mester, Diana Martins Bordalo, Ali Amr, Carsten Dietrich, Dietmar Pils, Dominik Siede, Hauke Hund, Andrea Bauer, Daniel Benjamin Holzer, Arjang Ruhparwar, Matthias Mueller-Hennessen, Dieter Weichenhan, Christoph Plass,

Tanja Weis, Johannes Backs, Maximilian Wuerstle, Andreas Keller, Hugo A. Katus, and Andreas E. Posch. Epigenome-wide association study identifies cardiac gene patterning and a novel class of biomarkers for heart failure. *Circulation*, 136(16):1528–1544, October 2017.

[95] Florence Momplaisir, Norrisa Haynes, Hervette Nkwihoreze, Maria Nelson, Rachel M Werner, and John Jemmott. Understanding drivers of coronavirus disease 2019 vaccine hesitancy among blacks. *Clinical Infectious Diseases*, 73(10):1784–1789, November 2021.

[96] T. Morasert, W. Worapas, R. Kaewmahit, and W. Uphala. Prevalence and risk factors associated with tuberculosis disease in Suratthani Central Prison, Thailand. *The International Journal of Tuberculosis and Lung Disease: The Official Journal of the International Union Against Tuberculosis and Lung Disease*, 22(10):1203–1209, October 2018.

[97] James O. Mudd and David A. Kass. Tackling heart failure in the twenty-first century. *Nature*, 451(7181):919–928, February 2008.

[98] C B Newgard, M J Brady, R M O'Doherty, and A R Saltiel. Organizing glucose disposal: emerging roles of the glycogen targeting subunits of protein phosphatase-1. *Diabetes*, 49(12):1967–1977, December 2000.

[99] Long H. Nguyen, Amit D. Joshi, David A. Drew, Jordi Merino, Wenjie Ma, Chun-Han Lo, Sohee Kwon, Kai Wang, Mark S. Graham, Lorenzo Polidori, Cristina Menni, Carole H. Sudre, Adjoa Anyane-Yeboa, Christina M. Astley, Erica T. Warner, Christina Y. Hu, Somesh Selvachandran, Richard Davies, Denis Nash, Paul W. Franks, Jonathan Wolf, Sebastien Ourselin, Claire J. Steves, Tim D. Spector, and Andrew T. Chan. Racial and ethnic differences in COVID-19 vaccine hesitancy and uptake. *medRxiv: The Preprint Server for Health Sciences*, page 2021.02.25.21252402, February 2021.

[100] Henry Njuguna, Megan Wallace, Sean Simonson, Farrell A. Tobolowsky, Allison E. James, Keith Bordelon, Rena Fukunaga, Jeremy A. W. Gold, Jonathan Wortham, Theresa Sokol, Danielle Haydel, Ha Tran, Kaylee Kim, Kiva A. Fisher, Mariel Marlow, Jacqueline E. Tate, Reena H. Doshi, and Kathryn G. Curran. Serial laboratory testing for sars-cov-2 infection among incarcerated and detained persons in a correctional and detention facility — louisiana, april–may 2020. *MMWR. Morbidity and Mortality Weekly Report*, 69(26):836–840, July 2020.

[101] D. Ojanuga. The medical ethics of the 'father of gynaecology', Dr J Marion Sims. *Journal of Medical Ethics*, 19(1):28–31, March 1993.

[102] A. David Paltiel, Jason L. Schwartz, Amy Zheng, and Rochelle P. Walensky. Clinical outcomes of a covid-19 vaccine: implementation over efficacy. *Health Affairs*, 40(1):42–52, January 2021.

[103] Tune H. Pers, Pascal Timshel, and Joel N. Hirschhorn. SNPsnap: a Web-based tool for identification and annotation of matched SNPs. *Bioinformatics*, 31(3):418–420, February 2015.

[104] Stephen Puleo. *A city so grand: the rise of an American metropolis, Boston 1850-1900*. Beacon Press, Boston, 2010. OCLC: ocn440563016.

[105] Eric Reinhart and Daniel L. Chen. Incarceration And Its Disseminations: COVID-19 Pandemic Lessons From Chicago's Cook County Jail: Study examines how arrest and pre-trial detention practices may be contributing to the spread of COVID-19. *Health Affairs*, 39(8):1412–1418, August 2020.

[106] Alicia R. Riley, Yea-Hung Chen, Ellicott C. Matthay, M. Maria Glymour, Jacqueline M. Torres, Alicia Fernandez, and Kirsten Bibbins-Domingo. Excess mortality among Latino people in California during the COVID-19 pandemic. *SSM - Population Health*, 15:100860, July 2021.

[107] Theresa Ryckman, Elizabeth T Chin, Lea Prince, David Leidner, Elizabeth Long, David M Studdert, Joshua A Salomon, Fernando Alarid-Escudero, Jason R Andrews, and Jeremy D Goldhaber-Fiebert. Outbreaks of COVID-19 variants in US prisons: a mathematical modelling analysis of vaccination and reopening policies. *The Lancet Public Health*, 6(10):e760–e770, October 2021.

[108] Brendan Saloner, Kalind Parish, Julie A. Ward, Grace DiLaura, and Sharon Dolovich. Covid-19 cases and deaths in federal and state prisons. *JAMA*, 324(6):602, August 2020.

[109] David B Savage, Lanmin Zhai, Balasubramanian Ravikumar, Cheol Soo Choi, Johanna E Snaar, Amanda C McGuire, Sung-Eun Wou, Gemma Medina-Gomez, Sheene Kim, Cheryl B Bock, Dyann M Segvich, Antonio Vidal-Puig, Nicholas J Wareham, Gerald I Shulman, Fredrik Karpe, Roy Taylor, Bartholomew A Pederson, Peter J Roach, Stephen O'Rahilly, and Anna A DePaoli-Roach. A prevalent variant in ppp1r3a impairs glycogen synthesis and reduces muscle glycogen content in humans and mice. *PLoS Medicine*, 5(1):e27, January 2008.

[110] Vahid Serpooshan, Senthilkumar Sivanesan, Xiaoran Huang, Morteza Mahmoudi, Andrey V. Malkovskiy, Mingming Zhao, Mohammed Inayathullah, Dhananjay Wagh, Xuexiang J. Zhang, Scott Metzler, Daniel Bernstein, Joseph C. Wu, Pilar Ruiz-Lozano, and Jayakumar Rajadas. [Pyr1]-Apelin-13 delivery via nano-liposomal encapsulation attenuates pressure overload-induced cardiac dysfunction. *Biomaterials*, 37:289–298, January 2015.

[111] Li Shen, Pardeep S. Jhund, Mark C. Petrie, Brian L. Claggett, Simona Barlera, John G. F. Cleland, Henry J. Dargie, Christopher B. Granger, John Kjekshus, Lars Køber, Roberto Latini, Aldo P. Maggioni, Milton Packer, Bertram Pitt, Scott D. Solomon, Karl Swedberg, Luigi Tavazzi, John Wikstrand, Faiez Zannad, Michael R. Zile, and John J. V. McMurray. Declining risk of sudden death in heart failure. *The New England Journal of Medicine*, 377(1):41–51, July 2017.

[112] Jamie Solis, Carlos Franco-Paredes, Andrés F. Henao-Martínez, Martin Krsak, and Shanta M. Zimmer. Structural vulnerability in the u. S. Revealed in three waves of covid-19. *The American Journal of Tropical Medicine and Hygiene*, 103(1):25–27, July 2020.

[113] Lin Song, Peter Langfelder, and Steve Horvath. Comparison of co-expression measures: mutual information, correlation, and model based indices. *BMC Bioinformatics*, 13(1):328, December 2012.

[114] Oliver Stegle, Leopold Parts, Matias Piipari, John Winn, and Richard Durbin. Using probabilistic estimation of expression residuals (Peer) to obtain increased power and interpretability of gene expression analyses. *Nature Protocols*, 7(3):500–507, March 2012.

[115] Rachel Strodel, Lauren Dayton, Henri M. Garrison-Desany, Gabriel Eber, Chris Beyrer, Joyell Arscott, Leonard Rubenstein, and Carolyn Sufrin. COVID-19 vaccine prioritization of incarcerated people relative to other vulnerable groups: An analysis of state plans. *PLOS ONE*, 16(6):e0253208, June 2021.

[116] Yoichi Suzuki, Carita Lanner, Jong-Hwa Kim, Pier Giuseppe Vilardo, Hong Zhang, Jie Yang, Lori D. Cooper, Marcella Steele, Andrew Kennedy, Cheryl B. Bock, Angus Scrimgeour, John C. Lawrence, and Anna A. DePaoli-Roach. Insulin control of glycogen metabolism in knockout mice lacking the muscle-specific protein phosphatase pp1g/r $_{gl}$. *Molecular and Cellular Biology*, 21(8):2683–2694, April 2001.

[117] Mark W. Tenforde, Samantha M. Olson, Wesley H. Self, H. Keipp Talbot, Christopher J. Lindsell, Jay S. Steingrub, Nathan I. Shapiro, Adit A. Ginde, David J. Douin, Matthew E. Prekker, Samuel M. Brown, Ithan D. Peltan, Michelle N. Gong, Amira Mohamed, Akram Khan, Matthew C. Exline, D. Clark Files, Kevin W. Gibbs, William B. Stubblefield, Jonathan D. Casey, Todd W. Rice, Carlos G. Grijalva, David N. Hager, Arber Shehu, Nida Qadir, Steven Y. Chang, Jennifer G. Wilson, Manjusha Gaglani, Kempapura Murthy, Nicole Calhoun, Arnold S. Monto, Emily T. Martin, Anurag Malani, Richard K. Zimmerman, Fernanda P. Silveira, Donald B. Middleton, Yuwei Zhu, Dayna Wyatt, Meagan Stephenson, Adrienne Baughman, Kelsey N. Womack, Kimberly W. Hart, Miwako Kobayashi, Jennifer R. Verani, Manish M. Patel, IVY Network, HAIVEN Investigators, IVY Network, Omowunmi Amosu, Brent Armbruster, Valerie Aston, Marianne Bernardo, Robert Bowers, Leslie De Souza, Jennifer Friedel, Kevin Gardner, Jennifer Goff, Alexandra June Gordon, Audrey Hendrickson, Madeline Hicks, Michelle Howell, Jakea Johnson, Jeffrey Jorgensen, Sarah Karow, Lori Kozikowski, Olivia Krol, Leigha Landreth, Mary LaRose, Brenda Lopez, New York, Andrea Luong, Bob McClellan, Ellen Maruggi, Karen Miller, Rahul Nair, Lisa Parks, Jennifer Peers, Cynthia Perez, Adreanne Rivera, Jonasel Roque, Andres Santana, Tyler Scharber, Emma Silverman, Michael Tozier, Hiwet Tzehaie, Zachary Zouyed, HAIVEN Investigators, Alejandro Arroliga, Alicia

Bagiatis, Gk Balasubramani, Caroline K. Cheng, Heather Eng, Shekhar Ghamande, Judy Herrick, Eric Hoffman, Kailey Hughes, Lois E. Lamerato, Adam S. Lauring, Amanda McKillop, Tresa McNeal, E.J. McSpadden, John Midturi, Manohar Mutnal, Mary Patricia Nowalk, Joshua G. Petrie, Chandni Raiyani, Arundhati Rao, Sean G. Saul, Theresa M. Sax, Hannah E. Segaloff, Lori Stiefel, Marcus Volz, Kimberly Walker, Nicole Wheeler, Heath White, John V. Williams, Mohamed Yassin, Martha Zayed, and Tnelda Zunie. Effectiveness of pfizer-biontech and moderna vaccines against covid-19 among hospitalized adults aged *geq*65 years — united states, january–march 2021. *MMWR. Morbidity and Mortality Weekly Report*, 70(18):674–679, May 2021.

[118] Stephen J. Thomas, Edson D. Moreira, Nicholas Kitchin, Judith Absalon, Alejandra Gurtman, Stephen Lockhart, John L. Perez, Gonzalo Pérez Marc, Fernando P. Polack, Cristiano Zerbini, Ruth Bailey, Kena A. Swanson, Xia Xu, Satrajit Roychoudhury, Kenneth Koury, Salim Bouguermouh, Warren V. Kalina, David Cooper, Robert W. Frenck, Laura L. Hammitt, Özlem Türeci, Haylene Nell, Axel Schaefer, Serhat Ünal, Qi Yang, Paul Liberator, Dina B. Tresnan, Susan Mather, Philip R. Dormitzer, Uğur Şahin, William C. Gruber, and Kathrin U. Jansen. Safety and efficacy of the bnt162b2 mrna covid-19 vaccine through 6 months. *New England Journal of Medicine*, 385(19):1761–1773, November 2021.

[119] Mark G. Thompson, Jefferey L. Burgess, Allison L. Naleway, Harmony Tyner, Sarang K. Yoon, Jennifer Meece, Lauren E.W. Olsho, Alberto J. Caban-Martinez, Ashley L. Fowlkes, Karen Lutrick, Holly C. Groom, Kayan Dunnigan, Marilyn J. Odean, Kurt Hegmann, Elisha Stefanski, Laura J. Edwards, Natasha Schaefer-Solle, Lauren Grant, Katherine Ellingson, Jennifer L. Kuntz, Tnelda Zunie, Matthew S. Thiese, Lynn Ivacic, Meredith G. Wesley, Julie Mayo Lamberte, Xiaoxiao Sun, Michael E. Smith, Andrew L. Phillips, Kimberly D. Groover, Young M. Yoo, Joseph Gerald, Rachel T. Brown, Meghan K. Herring, Gregory Joseph, Shawn Beitel, Tyler C. Morrill, Josephine Mak, Patrick Rivers, Brandon P. Poe, Brian Lynch, Yingtao Zhou, Jing Zhang, Anna Kelleher, Yan Li, Monica Dickerson, Erika Hanson, Kyley Guenther, Suxiang Tong, Allen Bateman, Erik Reisdorf, John Barnes, Eduardo Azziz-Baumgartner, Danielle R. Hunt, Melissa L. Arvay, Preeta Kutty, Alicia M. Fry, and Manjusha Gaglani. Prevention and Attenuation of Covid-19 with the BNT162b2 and mRNA-1273 Vaccines. *New England Journal of Medicine*, 385(4):320–329, July 2021.

[120] Cole Trapnell, Adam Roberts, Loyal Goff, Geo Pertea, Daehwan Kim, David R Kelley, Harold Pimentel, Steven L Salzberg, John L Rinn, and Lior Pachter. Differential gene and transcript expression analysis of RNA-seq experiments with TopHat and Cufflinks. *Nature Protocols*, 7(3):562–578, March 2012.

[121] Eva van Rooij, Lillian B. Sutherland, Ning Liu, Andrew H. Williams, John McAnally, Robert D. Gerard, James A. Richardson, and Eric N. Olson. A signature pattern of stress-responsive microRNAs that can evoke cardiac hypertrophy and heart failure. *Proceedings of the National Academy of Sciences of the United States of America*, 103(48):18255–18260, November 2006.

[122] Eleftheria Vasileiou, Colin R Simpson, Ting Shi, Steven Kerr, Utkarsh Agrawal, Ashley Akbari, Stuart Bedston, Jillian Beggs, Declan Bradley, Antony Chuter, Simon de Lusignan, Annemarie B Docherty, David Ford, FD Richard Hobbs, Mark Joy, Srinivasa Vittal Katikireddi, James Marple, Colin McCowan, Dylan McGagh, Jim McMenamin, Emily Moore, Josephine LK Murray, Jiafeng Pan, Lewis Ritchie, Syed Ahmar Shah, Sarah Stock, Fatemeh Torabi, Ruby SM Tsang, Rachael Wood, Mark Woolhouse, Chris Robertson, and Aziz Sheikh. Interim findings from first-dose mass COVID-19 vaccination roll-out and COVID-19 hospital admissions in Scotland: a national prospective cohort study. *The Lancet*, 397(10285):1646–1657, May 2021.

[123] Megan Wallace, Liesl Hagan, Kathryn G. Curran, Samantha P. Williams, Senad Handanagic, Adam Bjork, Sherri L. Davidson, Robert T. Lawrence, Joseph McLaughlin, Marilee Butterfield, Allison E. James, Naveen Patil, Kimberley Lucas, Justine Hutchinson, Lynn Sosa, Amanda Jara, Phillip Griffin, Sean Simonson, Catherine M. Brown, Stephanie Smoyer, Meghan Weinberg, Brittany Pattee, Molly Howell, Matthew Donahue, Soliman Hesham, Ellen Shelley, Grace Philips, David Selvage, E. Michele Staley, Anthony Lee, Mike Mannell, Orion McCotter, Raul Villalobos, Linda Bell, Abdoulaye Diedhiou, Dustin Ortbahn, Joshua L. Clayton, Kelsey Sanders, Hannah Cranford, Bree Barbeau, Katherine G. McCombs, Caroline Holsinger, Natalie A. Kwit, Julia C. Pringle, Sara Kariko, Lara Strick, Matt Allord, Courtney Tillman, Andrea Morrison, Devin Rowe, and Mariel Marlow. Covid-19 in correctional and detention facilities — united states, february–april 2020. *MMWR. Morbidity and Mortality Weekly Report*, 69(19):587–590, May 2020.

[124] Roddy Walsh, Kate L. Thomson, James S. Ware, Birgit H. Funke, Jessica Woodley, Karen J. McGuire, Francesco Mazzarotto, Edward Blair, Anneke Seller, Jenny C. Taylor, Eric V. Minikel, Exome Aggregation Consortium, Daniel G. MacArthur, Martin Farrall, Stuart A. Cook, and Hugh Watkins. Reassessment of Mendelian gene pathogenicity using 7,855 cardiomyopathy cases and 60,706 reference samples. *Genetics in Medicine*, 19(2):192–203, February 2017.

[125] Emily A. Wang, Bruce Western, and Donald M. Berwick. Covid-19, decarceration, and the role of clinicians, health systems, and payers: a report from the national academy of sciences, engineering, and medicine. *JAMA*, 324(22):2257, December 2020.

[126] Danielle Welter, Jacqueline MacArthur, Joannella Morales, Tony Burdett, Peggy Hall, Heather Junkins, Alan Klemm, Paul Flicek, Teri Manolio, Lucia Hindorff, and Helen Parkinson. The NHGRI GWAS Catalog, a curated resource of SNP-trait associations. *Nucleic Acids Research*, 42(Database issue):D1001–1006, January 2014.

[127] Bin Zhang, Chris Gaiteri, Liviu-Gabriel Bodea, Zhi Wang, Joshua McElwee, Alexei A. Podtelezhnikov, Chunsheng Zhang, Tao Xie, Linh Tran, Radu Dobrin, Eugene Fluder, Bruce Clurman, Stacey Melquist, Manikandan Narayanan, Christine Suver, Hardik Shah, Milind Mahajan, Tammy Gillis, Jayalakshmi Mysore, Marcy E. MacDonald, John R. Lamb, David A Bennett, Cliona Molony, David J. Stone, Vilmundur Gudnason, Amanda J. Myers, Eric E. Schadt, Harald Neumann, Jun Zhu, and Valur Emilsson. Integrated systems approach identifies genetic nodes and networks in late-onset Alzheimer's disease. *Cell*, 153(3):707–720, April 2013.

[128] Bin Zhang and Steve Horvath. A general framework for weighted gene co-expression network analysis. *Statistical Applications in Genetics and Molecular Biology*, 4(1), January 2005.

[129] Yuqi Zhao, Deepali Jhamb, Le Shu, Douglas Arneson, Deepak K. Rajpal, and Xia Yang. Multi-omics integration reveals molecular networks and regulators of psoriasis. *BMC systems biology*, 13(1):8, January 2019.